Enteropathogenic bacteria evade ROCK-driven epithelial cell extrusion

https://doi.org/10.1038/s41586-025-09645-0

Received: 30 August 2024

Accepted: 17 September 2025

Published online: 22 October 2025

Open access

Check for updates

Giovanni Luchetti[1]✉, Marin V. Miner[2], Rachael M. Peterson[2], William P. Scott[2], Praveen Krishnamoorthy[3], Eric M. Kofoed[4], Angel G. Jimenez[4], Hua Zhang[5], Man Wah Tan[4], Rohit Reja[6,7], Tommy K. Cheung[8], Elizabeth Skippington[9], Yuxin Liang[8], Christopher M. Rose[8], Nobuhiko Kayagaki[6], Kim Newton[6], Isabella Rauch[2]✉ & Vishva M. Dixit[6]✉

Diverse pathogen-encoded virulence factors disable apoptosis, pyroptosis or necroptosis, the host cell death programs that remove infected cells[1]. In the intestine, the extrusion of infected cells into the lumen for elimination provides an additional layer of host defence, but no virulence mechanisms that target the cytoskeletal changes required are known[2]. Here we show that the *Escherichia coli* ubiquitin ligase NleL is an inhibitor of intestinal epithelial cell (IEC) extrusion, targeting caspase-4, ROCK1 and ROCK2 for proteasomal degradation. Genetic deletion of *Rock1* and *Rock2* from cultured IECs diminished inflammasome-induced IEC extrusion. Moreover, mice with *Rock1*- and *Rock2*-deficient IECs were less effective than wild-type mice at constraining the numbers of *Citrobacter rodentium* in the colon. Notably, NleL-deficient *C. rodentium* triggered more IEC extrusion than did wild-type *C. rodentium*, resulting in diminished colonization of the colon in infected mice. Our work highlights a host–pathogen arms race focused on dynamic regulation of the host epithelial barrier.

The human protease caspase-4 and its mouse orthologue caspase-11 defend against gram-negative bacteria[3,4]. Activated by bacterial lipopolysaccharide (LPS) in the cytoplasm[5–7], caspase-4 and caspase-11 cleave and activate the pore-forming protein gasdermin D (GSDMD) to cause a lytic form of cell death called pyroptosis[8,9]. Eliminating infected cells in this manner denies microorganisms their replicative niche. Other bacterial components, including toxins and DNA, are sensed by intracellular inflammasome complexes that activate caspase-1, which also induces pyroptosis by cleaving GSDMD[1]. Pathogenic bacteria have evolved to thwart host defence mechanisms. For example, the intestinal pathogen *Shigella* evades pyroptosis in human cells because its ubiquitin ligase IpaH7.8 targets GSDMD and GSDMB for proteasomal degradation[10–12]. Granzyme A cleaves GSDMB to elicit pyroptosis when infected cells are targeted by cytotoxic lymphocytes[13]. Another *Shigella* effector, OspC3, suppresses pyroptosis by inhibiting caspase-4 and caspase-11 (refs. 14,15). Effectors from other pathogenic bacteria, including *Yersinia* YopM and *E. coli* NleA, suppress pyroptosis by inhibiting the activation of caspase-1 (refs. 16–18). *E. coli* NleF suppresses pyroptotic and apoptotic host cell death by inhibiting caspases 4, 8 and 9 (ref. 19).

NleL inhibits LPS-induced pyroptosis

To determine whether other virulence factors target host pyroptosis signalling, we screened 63 *E. coli* effectors (Extended Data Table 1) in a pooled format for their ability to block LPS-induced pyroptosis in human endothelial-like EA.hy926 cells (Extended Data Fig. 1a,b). Cells expressing doxycycline-induced *nleF* or *nleL* (also called *espX7* and encoded by two independent constructs in our lentiviral library) showed better survival after LPS transfection than did uninduced cells, and released less lactate dehydrogenase (LDH), which is a hallmark of lytic cell death (Fig. 1a,b). NleF is known to inhibit caspases, including caspase-4 (refs. 19,20), whereas NleL is a HECT-like E3 ubiquitin ligase that contributes to *C. rodentium* virulence in mice[21]. NleL is reported to ubiquitylate JUN N-terminal kinases (JNKs)[22] and IκB kinases (IKKs)[23]. Wild-type (WT) NleL suppressed LPS-induced cell death in EA.hy926 cells and human colonic Caco-2 cells, whereas catalytically inactive NleL(C735A) did not, despite being expressed more than WT NleL (Fig. 1c–e and Extended Data Fig. 1c,d). These data show that the ubiquitin ligase activity of NleL is required for its pro-survival function. Given that caspase-1- and GSDMD-dependent pyroptosis induced by Val-boroPro (VbP)[24] was unaffected by WT NleL (Fig. 1f), GSDMD is probably not the target of NleL.

Caspase-4 and ROCKs are NleL substrates

To identify NleL substrates in an unbiased manner, we used mass spectrometry to identify proteins with increased ubiquitylation after doxycycline-induced expression of NleL and decreased overall abundance (Extended Data Fig. 2a). The zinc-finger protein p66β, caspase-4 and the kinase ROCK2 showed the biggest increases in ubiquitylation

[1]Department of Discovery Oncology, Genentech, South San Francisco, CA, USA. [2]Department of Molecular Microbiology and Immunology, Oregon Health and Science University, Portland, OR, USA. [3]Department of Pathology, Genentech, South San Francisco, CA, USA. [4]Department of Immunology and Infectious Diseases, Genentech, South San Francisco, CA, USA. [5]Department of Translational Immunology, Genentech, South San Francisco, CA, USA. [6]Department of Physiological Chemistry, Genentech, South San Francisco, CA, USA. [7]Department of Oncology Bioinformatics, Genentech, South San Francisco, CA, USA. [8]Department of Proteomic and Genomic Technologies, Genentech, South San Francisco, CA, USA. [9]Department of OMNI Bioinformatics, Genentech, South San Francisco, CA, USA. ✉e-mail: luchettg@gene.com; rauchi@ohsu.edu; dixit@gene.com

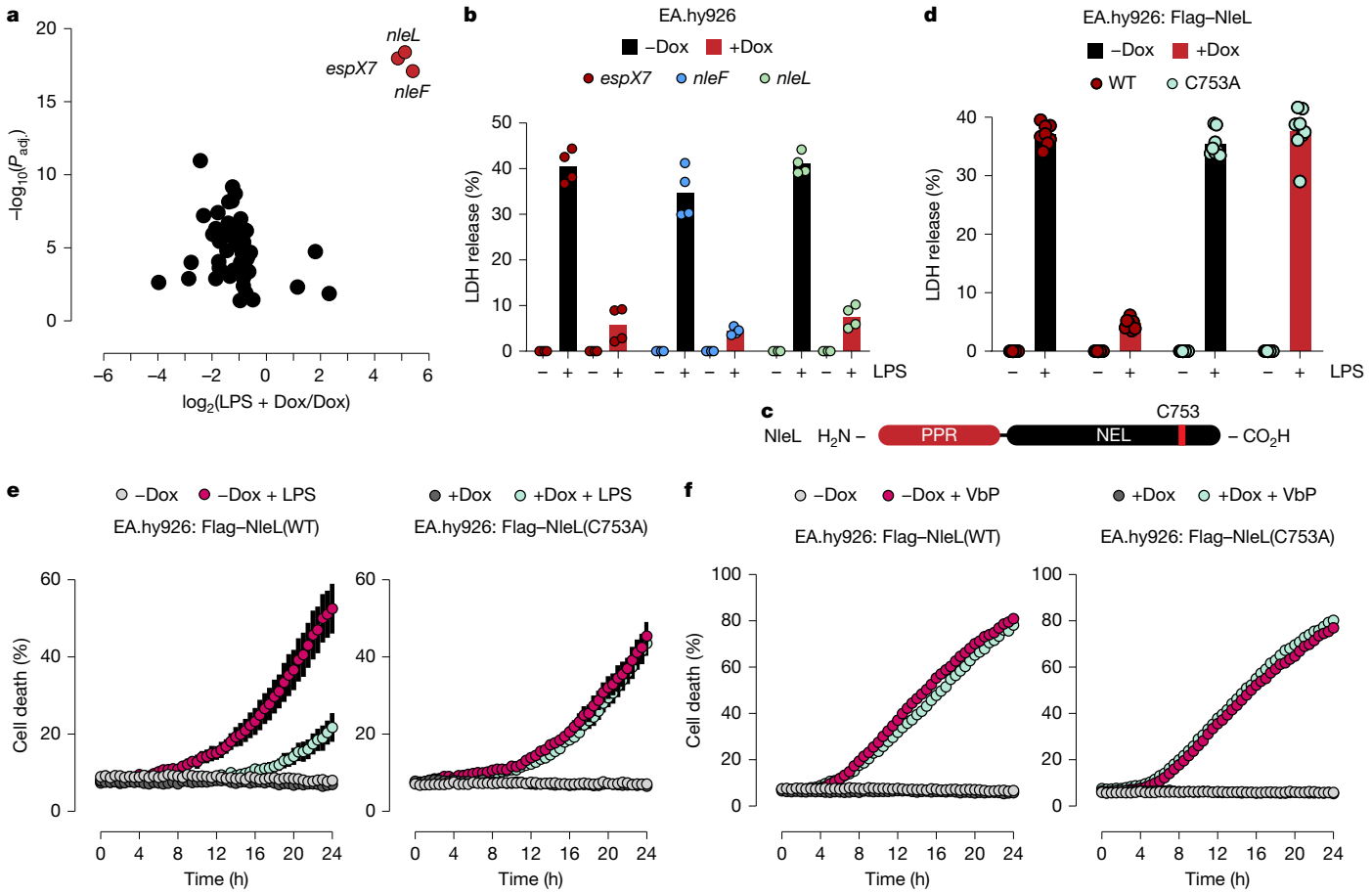

Fig. 1 | NleL ubiquitin ligase activity inhibits caspase-4-dependent pyroptosis. a, Changes in effector abundance after transfecting EA.hy926 cells with LPS. The *x* axis indicates the $\log_2$-transformed fold change in effector gene expression, and the *y* axis indicates the adjusted *P* value (two-sided Wald test, false discovery rate (FDR) adjustment by the Benjamini–Hochberg method; $n = 3$ per group). **b**,**d**, Percentage of LDH released from EA.hy926 cells at 24 h after LPS transfection. Where indicated, doxycycline (Dox) was used to induce effector expression. Circles indicate biological replicates ($n = 4$ (**b**) and $n = 8$ (**d**)). Bars indicate mean. **c**, Domain architecture of NleL, showing its essential catalytic Cys753, PPR and novel E3 ligase (NEL) domains. **e**,**f**, Kinetics of YOYO dye uptake by EA.hy926 cells after transfection with LPS (**e**) or treatment with 25 μM VbP (**f**). Data are mean (circles) ± s.d. (shaded area) of biological replicates ($n = 4$). Results in **b**,**d**–**f** are representative of three independent experiments.

in EA.hy926 cells between two hours and six hours after NleL induction (Fig. 2a). Caspase-4 residues Lys87 and Lys293 were modified at one hour after doxycycline treatment, but the total amount of caspase-4 declined at two hours, consistent with ubiquitylation-induced protein degradation (Fig. 2b). The levels of other caspases, including caspase-1, were unaffected by NleL (Extended Data Fig. 2b). NleL-induced ROCK2 ubiquitylation also coincided with a drop in the total amount of ROCK2 (Fig. 2c). We did not detect ubiquitylation of the related kinase ROCK1, but its decline in cells expressing NleL suggested that ROCK1 and ROCK2 might both be NleL substrates (Extended Data Fig. 2c). Reported NleL substrates[22,23] JNK1, JNK2, IKKα, IKKβ, TRAF2 and TRAF6 were not reduced or ubiquitylated by NleL expression in EA.hy926 cells (Extended Data Fig. 2d–f).

Western blotting confirmed that WT NleL suppressed endogenous caspase-4 and ROCK2 protein expression in EA.hy926, Caco-2 and human colorectal HT-29 cells, whereas NleL(C753A) did not (Fig. 2d and Extended Data Fig. 2g,h). Endogenous ROCK1 protein expression in HT-29 cells was also reduced by WT NleL, but not by NleL(C753A) (Extended Data Fig. 2g). By contrast, the suppressive effect of NleL on p66β expression in EA.hy926 cells was also seen with NleL(C753A) (Fig. 2d). Moreover, the levels of p66β in HT-29 cells were unaffected by NleL (Extended Data Fig. 2g). Collectively, these results argue against p66β being a direct substrate of NleL. Hereafter, we focus on NleL's regulation of caspase-4 and the ROCKs.

The disappearance of caspase-4 and ROCK2 from EA.hy926 and Caco-2 cells expressing NleL was prevented by the ubiquitin-activating enzyme 1 (UAE1) inhibitor MLN7243 or the proteasome inhibitor bortezomib (Fig. 2e and Extended Data Fig. 2i), consistent with NleL targeting caspase-4 and ROCK2 for proteasomal degradation. Caspase-4 bearing K48-linked polyubiquitin chains accumulated in bortezomib-treated cells expressing NleL (Extended Data Fig. 2j), indicating that this species is targeted for degradation. This result is consistent with studies showing that NleL builds K6- and K48-linked polyubiquitin[25,26]. The degradation of caspase-4 explains the resistance of NleL-expressing cells to LPS-induced pyroptosis. Note that WT NleL—but not NleL(C753A)—also induced the disappearance of co-transfected mouse caspase-11 (Extended Data Fig. 2k). Thus, NleL would be expected to inhibit LPS-induced pyroptosis in mouse and human cells.

The *Salmonella* HECT-like E3 ubiquitin ligase SopA, a close homologue of NleL[27], served as a negative control in subsequent biochemical studies. Unlike NleL, SopA did not cause the disappearance of co-transfected caspase-4 (Fig. 2f) or ROCK2 (Fig. 2g). Notably, catalytically inactive NleL(C753A) co-immunoprecipitated with co-transfected caspase-4, ROCK2 or ROCK1, whereas catalytically inactive SopA(C753A) did not (Fig. 2h,i and Extended Data Fig. 2l–n). Consistent with caspase-4, ROCK2 and ROCK1 being direct substrates of NleL, purified caspase-4, ROCK2 and ROCK1 were ubiquitylated in vitro by purified WT NleL, but not by NleL(C753A) (Fig. 2j,k and Extended Data Fig. 2o,p).

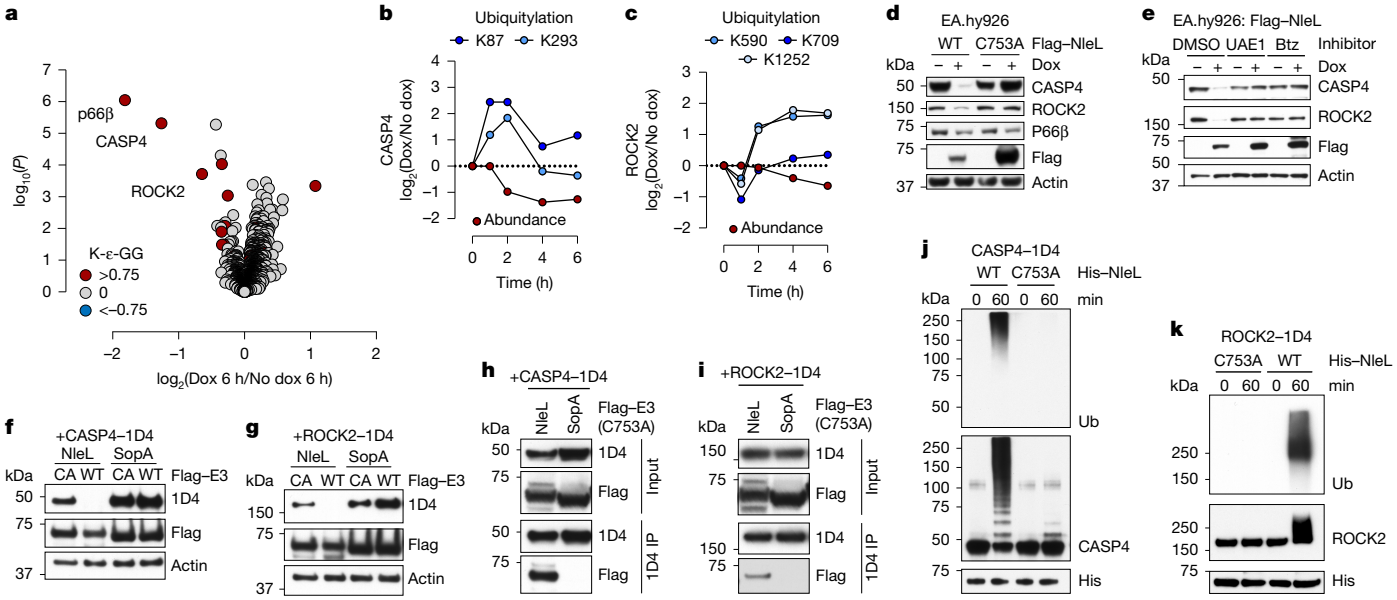

Fig. 2 | Caspase-4, ROCK1 and ROCK2 are NleL substrates. a, Changes in total protein abundance (*x* axis) and K-ε-GG peptide abundance (circle colour) after six hours of doxycycline (Dox)-induced NleL expression in EA.hy926 cells. *P* values determined by two-sided Student's *t*-test; $n = 2$ per group. **b**,**c**, Changes in total caspase-4 (**b**) and ROCK2 (**c**) abundance (red circles) and their peptides bearing ubiquitylated lysines (blue circles) in EA.hy926 cells after doxycycline-induced NleL expression. Data are mean of biological replicates ($n = 2$). **d**,**e**, Immunoblots of EA.hy926 cells. Where indicated, cells were transfected with WT or catalytically inactive NleL (**d**) or treated for four hours with dimethyl sulfoxide (DMSO) vehicle or 1 μM bortezomib (Btz) or UAE1 inhibitor (**e**). Results are representative of three independent experiments. **f**,**g**, Immunoblots of 293T cells transfected with 1D4-tagged caspase-4 (**f**) or 1D4-tagged ROCK2 (**g**) and Flag-tagged bacterial E3 ligases. CA, NleL(C753A). Results are representative of three independent experiments. **h**,**i**, Immunoblots of 1D4-tagged caspase-4 (**h**) or 1D4-tagged ROCK2 (**i**) complexes with Flag-tagged E3 ligases NleL(C753A) or SopA immunoprecipitated (IP) from transfected 293T cells. Results are representative of three independent experiments. **j**,**k**, Immunoblots of in vitro ubiquitylation reactions using caspase-4 (**j**) or ROCK2 (**k**) as NleL substrates. Ub, ubiquitin. Results are representative of three independent experiments. For gel source data, see Supplementary Fig. 1.

NleL targets LPS-sensing CARDs

Deleting the N-terminal caspase activation and recruitment domain (CARD) in caspase-4 prevented its ubiquitylation by NleL and subsequent degradation (Fig. 3a and Extended Data Fig. 3a). A CARD-less caspase-11 was also insensitive to NleL-induced degradation (Extended Data Fig. 3b), suggesting that an LPS-sensing CARD conferred susceptibility to NleL. Accordingly, the CARDs of caspases 4, 5 and 11 were detected in cells that co-expressed NleL(C753A), but not in those that co-expressed WT NleL (Fig. 3b). By contrast, the CARDs of 33 other proteins (Extended Data Table 2), including caspases 1, 2 and 9, were readily detected when co-expressed with WT NleL (Fig. 3c and Extended Data Fig. 3c). Of note, the selectivity of NleL for the LPS-sensing CARDs did not stem from it failing to bind to the other CARDs. NleL(C753A) interacted with the CARD of caspase-1 as well as with that of caspases 4, 5 and 11 (Extended Data Fig. 3d). A precise understanding of how the interaction of NleL with the LPS-sensing CARD of caspases 4, 5 or 11 results in ubiquitylation will require more detailed structural information.

To determine whether an LPS-sensing CARD would confer NleL susceptibility on caspase-1, we replaced the CARD in caspase-1 with that of caspase-4, and vice versa (Extended Data Fig. 3e). The caspase-4 CARD rendered caspase-1 sensitive to NleL-induced degradation, and, by contrast, the caspase-1 CARD made caspase-4 resistant. Substituting caspase-1 residues 6–20 with those from caspase-4 also sensitized caspase-1 to regulation by NleL (Fig. 3c and Extended Data Fig. 3f). In addition, residues 6–20 from the caspase-1 CARD neutralized NleL regulation when placed in caspase-4 (Fig. 3c and Extended Data Fig. 3g). Although we were unable to precisely define the motif within the caspase-4 CARD that confers NleL susceptibility, AlphaFold modelling of the caspase-1 and caspase-4 CARDs highlighted distinct structural properties that correlated with proteasomal degradation. The model of the caspase-1 CARD shows the canonical bundle of six antiparallel helices characteristic of death-fold proteins, whereas the model of the caspase-4 CARD does not (Extended Data Fig. 3h).

NleL targets the PH domain in ROCK2

ROCK1 and ROCK2 do not contain a CARD, so it was unclear which domain rendered them susceptible to NleL. Truncations of ROCK2 indicated that the C-terminal pleckstrin homology (PH) domain was necessary and sufficient for instability in cells expressing WT NleL (Fig. 3f). Deleting the last 20 residues of ROCK2 also stabilized the protein in NleL-expressing cells (Fig. 3g and Extended Data Fig. 4a). In keeping with these data, the purified PH domain of ROCK2 was ubiquitylated by NleL in vitro, but the kinase domain was not (Extended Data Fig. 4b,c).

The N-terminal pentapeptide repeat (PPR) domain in SopA has been shown[28] to bind to the SopA substrates TRIM56 and TRIM65. The NleL PPR domain, either alone or together with the ubiquitin ligase N lobe (PRR-N), co-immunoprecipitated with caspase-4 and ROCK2, whereas the ubiquitin ligase C lobe (NEL-C) did not (Fig. 3f and Extended Data Fig. 4d–g). Thus, the NleL PPR domain, like the SopA PPR domain, contributes to substrate binding. Notably, the NEL domain, composed of the N and C lobes, also interacted with caspase-4, ROCK2 and ROCK1 (Extended Data Fig. 4d–g), indicating that the N lobe must participate in substrate binding too. N-terminal truncations of the NEL domain suggested that residues between Glu372 and Gly486 mediated interactions with caspase-4 (Extended Data Fig. 4h).

NleL limits ROCK-driven IEC extrusion

To confirm that NleL targets caspase-4 and ROCK2 for degradation during an actual infection, we infected Caco-2 cells with the enterohaemorrhagic *E. coli* (EHEC) O157:H7 strain EDL933 or with a derivative

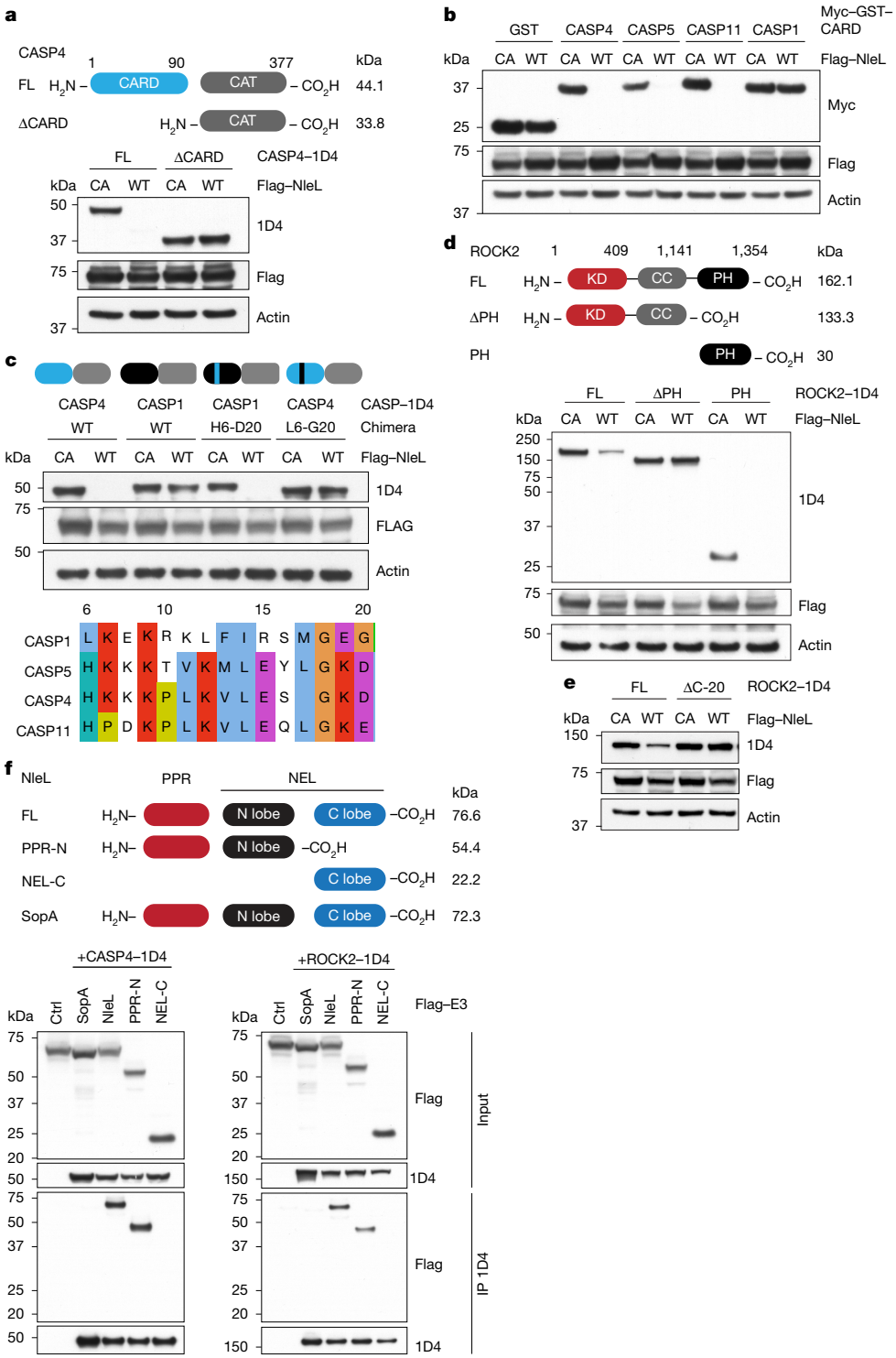

Fig. 3 | NleL targets the CARD in caspase-4, caspase-5 and caspase-11, and the PH domain in ROCK2. a–**d**, Immunoblots of 293T cells transfected with the constructs indicated. FL, full length. The domain architecture of caspase-4 with the CARD and catalytic (CAT) subunits is shown in **a**. In **b**, only the CARDs of the indicated caspases are expressed. Caspase residues 6–20 are aligned in **c**. The domain architecture of ROCK2 with the kinase domain (KD), coiled coil domain (CC) and PH domain is depicted in **d**. **e**, Immunoblots of 293T cells transfected with the constructs indicated. ΔC-20, ROCK2 20 aa C-terminal truncation. **f**, Immunoblots of 293T cells transfected with the constructs indicated. The domain architecture of NleL with PPR domain and catalytic N lobe (PPR-N), catalytic C-terminal domain (C lobe) and homologue SopA is depicted. Results are representative of three independent experiments. For gel source data, see Supplementary Fig. 1.

lacking NleL (Δ*nleL*). Western blotting revealed an NleL-dependent reduction in caspase-4 and ROCK2 at two hours and at four hours after infection, respectively (Fig. 4a). The loss of caspase-4 and ROCK2 from cells infected with the WT parental strain was prevented by bortezomib (Fig. 4b), indicating that both proteins were degraded in the proteasome. Of note, NleL-dependent changes in the abundance of ROCK2 coincided with altered ROCK signalling. Infection with Δ*nleL* EHEC elicited more phosphorylation of the ROCK substrate myosin light

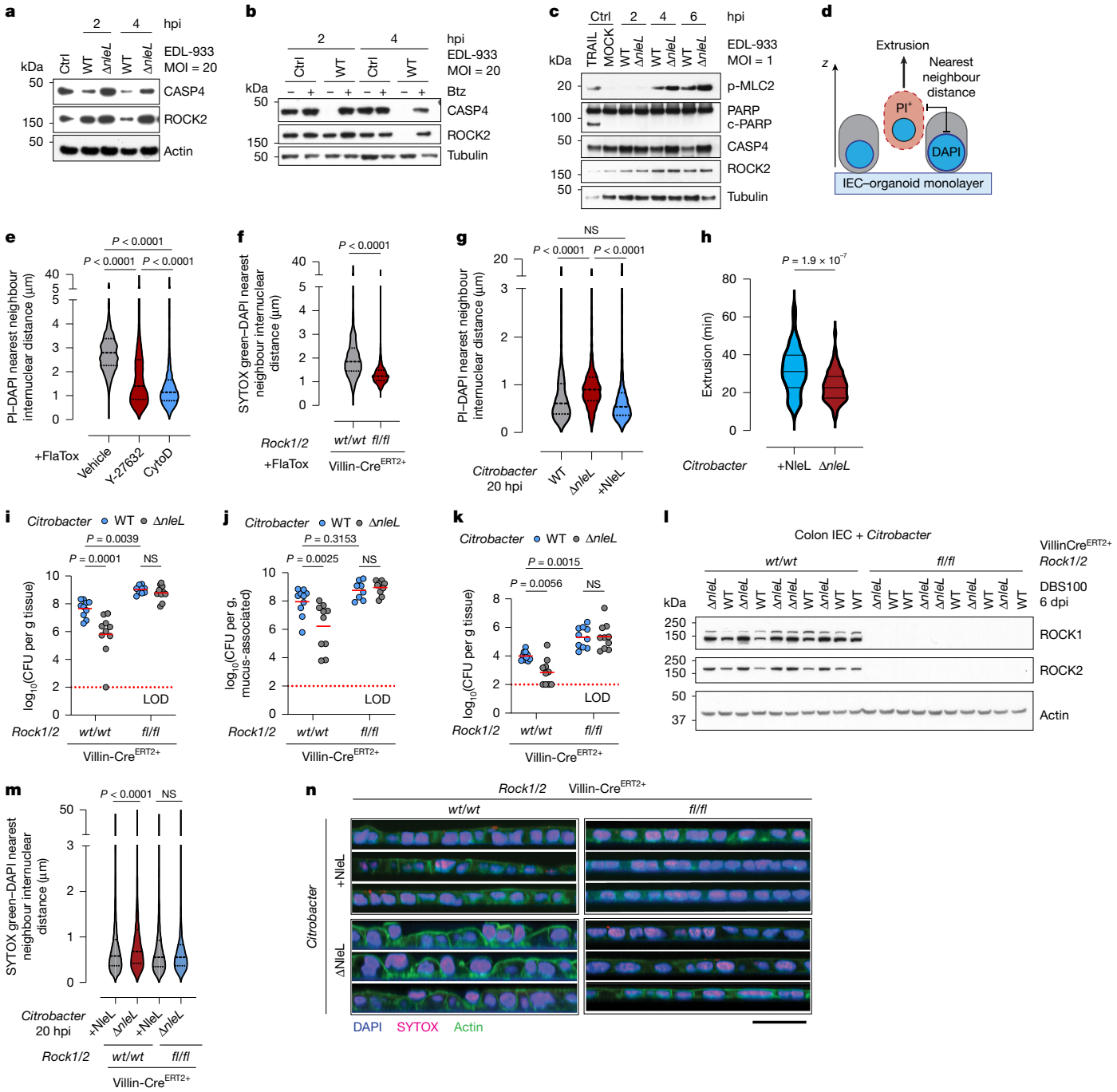

Fig. 4 | NleL limits the ROCK-dependent expulsion of IECs. a–**c**, Immunoblots of Caco-2 cells infected by *E. coli* strain EDL933. Infection with WT or NleL deficient strains (**a**). Where indicated, cells were cultured in 1 μM bortezomib (Btz) (**b**) or 10 μg ml^{-1} TRAIL (**c**). hpi, hours post-infection. Results are representative of three independent experiments. MOI, multiplicity of infection; p, phosphorylated; c, cleaved. **d**, Scheme for quantifying the cellular extrusion of dead PI$^+$ IECs from monolayers. **e**–**g**,**m**, Nearest neighbour internuclear distances in IEC monolayers. **e**, Cells from WT IEC organoids were treated for 30 min with FlaTox and DMSO vehicle, 2.5 mM cytochalasin D (CytoD) or 10 μM Y-27632. $n = 8$ monolayers per group. **f**, Cells from *Rock1*- and *Rock2*-knockout IEC organoids were stimulated with FlaTox. $n = 4$ monolayers per group. **g**,**m**, Cells from WT (**g**) or Villin.CreERT2 control and *Rock1*- and *Rock2*-knockout (**m**) IEC organoids were infected with *Citrobacter* strain DBS100 (WT, Δ*nleL* or +NleL). $n = 4$ monolayers per group. *P* values determined by two-tailed Mann–Whitney test. NS, not significant. Results are representative of three independent experiments. **h**, Quantification of extrusion time of individual cells in live-imaged WT IEC monolayers infected with *Citrobacter* strain DBS100 (Δ*nleL* or +NleL). *P* values determined by two-tailed Mann–Whitney test. Results are representative of two independent experiments. **i**–**k**, Colony-forming units (CFUs) in the mouse colon (**i**), colon lumen (**j**) and spleen (**k**) six days after infection with *Citrobacter* strain DBS100. Circles, different mice (data pooled from two experiments, $n = 10$ mice per group); lines, mean. *P* values determined by two-way ANOVA. LOD, limit of detection. **l**, Immunoblots of colon IECs from mice infected by *Citrobacter* strain DBS100. Results are representative of three independent experiments. **n**, Representative confocal *z*-stacks of the IEC cultures in **m**. Scale bar, 30 μm. For gel source data, see Supplementary Fig. 1.

chain 2 (MLC2) than did infection with WT EHEC (Fig. 4c). These data are consistent with the idea that NleL counters infection-induced ROCK–MLC2 signalling.

Inflammasome activation in *Salmonella*-infected IECs promotes pyroptosis and extrusion of the dying cells into the gut lumen[2,29]. Given that ROCK1 and ROCK2 mediate cytoskeletal rearrangements in dying

cells[30–33], we wondered whether ROCK1 and/or ROCK2 contribute to the extrusion of infected IECs. We investigated this possibility in monolayers of primary mouse IECs that were treated with FlaTox to activate the NAIP–NLRC4 inflammasome[34]. The membrane-impermeable dye propidium iodide (PI) was used to identify dying IECs being extruded from the monolayer (Fig. 4d). The ROCK1 and ROCK2 selective inhibitor Y-27632 impaired FlaTox-induced IEC extrusion from organoid monolayers, as did cytochalasin D, an inhibitor of actin polymerization (Fig. 4e). Genetic deletion of *Rock1* and *Rock2* from IECs also reduced FlaTox-induced IEC extrusion (Fig. 4f). Collectively, these data indicate that ROCK1 and/or ROCK2 promote the ejection of pyroptotic cells from IEC monolayers.

To determine whether NleL interferes with this process by targeting ROCK1 and ROCK2 for degradation, we infected IEC monolayers with the *C. rodentium* strain DBS100 or a Δ*nleL* derivative. In 293T cells, NleL reduced the expression of co-transfected mouse ROCK1 and ROCK2 to the same extent as it did for human ROCK1 and ROCK2 (Extended Data Fig. 5a). Monolayers infected with Δ*nleL Citrobacter* showed significantly increased extrusion at 20 h after infection, compared with those infected with the WT parental strain (Fig. 4g). Moreover, reconstituting NleL expression in Δ*nleL Citrobacter* normalized IEC extrusion to that seen with the WT parental strain. All bacteria in these experiments expressed GFP, which enabled us to enumerate bacteria adhering to IECs, and to ensure PI staining coincided with bacterial infection. *nleL* deficiency did not alter the number of adhered bacteria (Extended Data Fig. 5b). Moreover, more than 90% of PI-positive cells fell within the cellular radius of a GFP-positive bacterium (Extended Data Fig. 5c), and infection was required to promote measurable PI uptake (Extended Data Fig. 5d). In live-imaged monolayers, those infected with Δ*nleL Citrobacter* showed a higher rate of extrusion than did those infected by the strain complemented by NleL expression (Fig. 4h and Extended Data Fig. 5e).

To assess the role of the ROCKs during an infection in vivo, we used *Rock1*$^{fl/fl}$*Rock2*$^{fl/fl}$ Villin.CreERT2 mice, which permit the tamoxifen-inducible deletion of *Rock1* and *Rock2* specifically in IECs[35]. Western blotting of colonic IECs from *Rock1*$^{fl/fl}$*Rock2*$^{fl/fl}$ Villin.CreERT2 mice after treatment with tamoxifen confirmed that ROCK1 and ROCK2 were eliminated (Extended Data Fig. 5f). Of note, ROCK deficiency in IECs did not increase intestinal permeability to a high-molecular-weight fluorescein isothiocyanate (FITC)–dextran (Extended Data Fig. 5g), indicating that the intestinal barrier remained intact. When tamoxifen-treated *Rock1*$^{fl/fl}$*Rock2*$^{fl/fl}$ Villin.CreERT2 and Villin.CreERT2 mice were infected with WT *Citrobacter* for ten days, the former had significantly more bacteria in their colonic epithelium than did the latter (Extended Data Fig. 5h), consistent with ROCK1 and/or ROCK2 contributing to a host defence mechanism that suppresses bacterial numbers. When WT C57BL/6 mice were infected with WT or Δ*nleL Citrobacter* for six days, the WT *Citrobacter* was more abundant in the colon than the Δ*nleL* strain was (Extended Data Fig. 5i), consistent with NleL suppressing the extrusion of infected cells.

If ROCK1 and ROCK2 are crucial substrates of NleL, then WT and Δ*nleL Citrobacter* should exhibit comparable colonization of colons that already lack ROCK1 and ROCK2. Therefore, we next compared WT and Δ*nleL Citrobacter* colonization in tamoxifen-treated *Rock1*$^{fl/fl}$ *Rock2*$^{fl/fl}$ Villin.CreERT2 and Villin.CreERT2 mice at six days after infection. Consistent with our previous results in WT mice six days after infection (Extended Data Fig. 5i), Δ*nleL Citrobacter* exhibited a colonization defect in Villin.CreERT2 control mice, when compared with WT *Citrobacter* (Fig. 4i,j and Extended Data Fig. 5j). This defect was not evident in mice with *Rock*-deficient intestines (Fig. 4i,j and Extended Data Fig. 5j), consistent with NleL targeting the ROCKs to promote bacterial colonization. We also found that the dissemination of Δ*nleL Citrobacter* to the spleen was impaired in Villin.CreERT2 mice, but not in *Rock1*$^{fl/fl}$ *Rock2*$^{fl/fl}$ Villin.CreERT2 mice, further validating the importance of this virulence mechanism (Fig. 4k). By western blotting, colonic IECs from Villin.CreERT2 mice infected with WT *Citrobacter* contained less ROCK1 and ROCK2 than did those from Villin.CreERT2 mice infected with Δ*nleL Citrobacter*, providing biochemical evidence of NleL-dependent degradation of ROCK in vivo (Fig. 4l).

Consistent with our in vivo data, Δ*nleL Citrobacter* induced the extrusion of control but not ROCK-deficient IECs in cultured monolayers (Fig. 4m,n). Although NleL might target caspase-4 to limit pyroptosis upstream of ROCK-dependent IEC extrusion, IECs infected with Δ*nleL Citrobacter* did not secrete more interleukin-18 (IL-18) or exhibit more cell death than did those infected with WT *Citrobacter* (Extended Data Fig. 5k,l). This result was unsurprising because WT and Δ*nleL Citrobacter* can both express the caspase inhibitor NleF to suppress pyroptosis. In other control experiments, Villin.CreERT2 and *Rock*-deficient Villin.CreERT2 IEC monolayers exhibited equivalent resistance in a transepithelial electrical resistance assay (Extended Data Fig. 5m), indicating that *Rock* deficiency alone does not compromise the integrity of the IEC monolayer.

Collectively, our findings identify ROCK1 and/or ROCK2 as key targets of the NleL ubiquitin ligase in establishing a productive infection in the intestine.

Conclusion

By targeting caspases 4, 5 and 11 as well as ROCK1 and ROCK2 for proteasomal degradation, NleL has two opportunities to combat the pyroptotic elimination of infected IECs. Eliminating the caspases would prevent any pyroptotic response to cytosolic bacterial LPS, whereas eliminating ROCK1 and ROCK2 is most likely to hinder the extrusion of dying infected cells through the faeces. The caspase and ROCK residues required for ubiquitylation by NleL are quite different at the primary sequence level, implying different modes of substrate recognition. Structural studies of NleL in complex with its substrates might shed light on how these regions promote substrate ubiquitylation.

Online content

Any methods, additional references, Nature Portfolio reporting summaries, source data, extended data, supplementary information, acknowledgements, peer review information; details of author contributions and competing interests; and statements of data and code availability are available at https://doi.org/10.1038/s41586-025-09645-0.

1. Newton, K., Strasser, A., Kayagaki, N. & Dixit, V. M. Cell death. *Cell* **187**, 235–256 (2024).
2. Rauch, I. et al. NAIP-NLRC4 inflammasomes coordinate intestinal epithelial cell extrusion with eicosanoid and IL-18 release via activation of caspase-1 and -8. *Immunity* **46**, 649–659 (2017).
3. Aachoui, Y. et al. Caspase-11 protects against bacteria that escape the vacuole. *Science* **339**, 975–978 (2013).
4. Casson, C. N. et al. Human caspase-4 mediates noncanonical inflammasome activation against gram-negative bacterial pathogens. *Proc. Natl Acad. Sci. USA* **112**, 6688–6693 (2015).
5. Kayagaki, N. et al. Noncanonical inflammasome activation by intracellular LPS independent of TLR4. *Science* **341**, 1246–1249 (2013).
6. Hagar, J. A., Powell, D. A., Aachoui, Y., Ernst, R. K. & Miao, E. A. Cytoplasmic LPS activates caspase-11: implications in TLR4-independent endotoxic shock. *Science* **341**, 1250–1253 (2013).
7. Shi, J. et al. Inflammatory caspases are innate immune receptors for intracellular LPS. *Nature* **514**, 187–192 (2014).
8. Kayagaki, N. et al. Caspase-11 cleaves gasdermin D for non-canonical inflammasome signalling. *Nature* **526**, 666–671 (2015).
9. Shi, J. et al. Cleavage of GSDMD by inflammatory caspases determines pyroptotic cell death. *Nature* **526**, 660–665 (2015).
10. Hansen, J. M. et al. Pathogenic ubiquitination of GSDMB inhibits NK cell bactericidal functions. *Cell* **184**, 3178–3191 (2021).
11. Luchetti, G. et al. *Shigella* ubiquitin ligase IpaH7.8 targets gasdermin D for degradation to prevent pyroptosis and enable infection. *Cell Host Microbe* **29**, 1521–1530 (2021).
12. Wang, C. et al. Structural basis for GSDMB pore formation and its targeting by IpaH7.8. *Nature* **616**, 590–597 (2023).
13. Zhou, Z. et al. Granzyme A from cytotoxic lymphocytes cleaves GSDMB to trigger pyroptosis in target cells. *Science* **368**, eaaz7548 (2020).
14. Kobayashi, T. et al. The *Shigella* OspC3 effector inhibits caspase-4, antagonizes inflammatory cell death, and promotes epithelial infection. *Cell Host Microbe* **13**, 570–583 (2013).

15. Li, Z. et al. *Shigella* evades pyroptosis by arginine ADP-riboxanation of caspase-11. *Nature* **599**, 290–295 (2021).
16. LaRock, C. N. & Cookson, B. T. The *Yersinia* virulence effector YopM binds caspase-1 to arrest inflammasome assembly and processing. *Cell Host Microbe* **12**, 799–805 (2012).
17. Yen, H., Sugimoto, N. & Tobe, T. Enteropathogenic *Escherichia coli* uses NleA to inhibit NLRP3 inflammasome activation. *PLoS Pathog.* **11**, e1005121 (2015).
18. Ratner, D. et al. The *Yersinia pestis* effector YopM inhibits pyrin inflammasome activation. *PLoS Pathog.* **12**, e1006035 (2016).
19. Blasche, S. et al. The *E. coli* effector protein NleF is a caspase inhibitor. *PLoS ONE* **8**, e58937 (2013).
20. Pallett, M. A. et al. Bacterial virulence factor inhibits caspase-4/11 activation in intestinal epithelial cells. *Mucosal Immunol.* **10**, 602–612 (2017).
21. Piscatelli, H. et al. The EHEC type III effector NleL is an E3 ubiquitin ligase that modulates pedestal formation. *PLoS ONE* **6**, e19331 (2011).
22. Sheng, X. et al. Bacterial effector NleL promotes enterohemorrhagic *E. coli*-induced attaching and effacing lesions by ubiquitylating and inactivating JNK. *PLoS Pathog.* **13**, e1006534 (2017).
23. Sheng, X. et al. Enterohemorrhagic *E. coli* effector NleL disrupts host NF-κB signaling by targeting multiple host proteins. *J. Mol. Cell. Biol.* **12**, 318–321 (2020).
24. Okondo, M. C. et al. DPP8 and DPP9 inhibition induces pro-caspase-1-dependent monocyte and macrophage pyroptosis. *Nat. Chem. Biol.* **13**, 46–53 (2017).
25. Lin, D. Y., Diao, J., Zhou, D. & Chen, J. Biochemical and structural studies of a HECT-like ubiquitin ligase from *Escherichia coli* O157:H7. *J. Biol. Chem.* **286**, 441–449 (2011).
26. Hospenthal, M. K., Freund, S. M. & Komander, D. Assembly, analysis and architecture of atypical ubiquitin chains. *Nat. Struct. Mol. Biol.* **20**, 555–565 (2013).
27. Lin, D. Y., Diao, J. & Chen, J. Crystal structures of two bacterial HECT-like E3 ligases in complex with a human E2 reveal atomic details of pathogen-host interactions. *Proc. Natl Acad. Sci. USA* **109**, 1925–1930 (2012).
28. Fiskin, E. et al. Structural basis for the recognition and degradation of host TRIM proteins by *Salmonella* effector SopA. *Nat. Commun.* **8**, 14004 (2017).
29. Sellin, M. E. et al. Epithelium-intrinsic NAIP/NLRC4 inflammasome drives infected enterocyte extrusion to restrict *Salmonella* replication in the intestinal mucosa. *Cell Host Microbe* **16**, 237–248 (2014).
30. Sebbagh, M. et al. Caspase-3-mediated cleavage of ROCK I induces MLC phosphorylation and apoptotic membrane blebbing. *Nat. Cell Biol.* **3**, 346–352 (2001).
31. Coleman, M. L. et al. Membrane blebbing during apoptosis results from caspase-mediated activation of ROCK I. *Nat. Cell Biol.* **3**, 339–345 (2001).
32. Sebbagh, M., Hamelin, J., Bertoglio, J., Solary, E. & Breard, J. Direct cleavage of ROCK II by granzyme B induces target cell membrane blebbing in a caspase-independent manner. *J. Exp. Med.* **201**, 465–471 (2005).
33. Marchiando, A. M. et al. The epithelial barrier is maintained by in vivo tight junction expansion during pathologic intestinal epithelial shedding. *Gastroenterology* **140**, 1208–1218 (2011).
34. Scott, W. P. & Rauch, I. Inducing pyroptosis with FlaTox, RodTox, or NeedleTox. *Methods Mol. Biol.* **2641**, 27–36 (2023).
35. Sambandam, A. et al. Obligate role for Rock1 and Rock2 in adult stem cell viability and function. *Heliyon* **9**, e14238 (2023).

Methods

Mice

All mouse studies complied with relevant ethics regulations and were approved by either the Genentech Institutional Animal Care and Use Committee (IACUC) in an Association for Assessment and Accreditation of Laboratory Animal Care (AAALAC)-accredited facility or by the Oregon Health and Science University IACUC. Mice were housed in individually ventilated cages within animal rooms maintained on a 14-h–10-h light–dark cycle. Animal rooms were temperature and humidity controlled, at 20–26 °C and 30–70%, respectively, with 10–15 exchanges of air in the room per hour. *Rock1*$^{fl/fl}$*Rock2*$^{fl/fl}$ Villin.creERT2 mice on a C57BL/6J genetic background have been described previously[35]. Experimental cohorts of female mice were generated through two rounds of breeding: first *Rock1*$^{fl/+}$*Rock2*$^{fl/+}$ Villin.creERT2 mice were crossed to *Rock1*$^{fl/+}$*Rock2*$^{fl/+}$ mice, and then their offspring were bred together (either *Rock1*$^{fl/fl}$*Rock2*$^{fl/fl}$ Villin.creERT2 × *Rock1*$^{fl/fl}$*Rock2*$^{fl/fl}$ or *Rock1*$^{+/+}$*Rock2*$^{+/+}$ Villin.creERT2 × *Rock1*$^{+/+}$*Rock2*$^{+/+}$). Before infection with *C. rodentium* DBS100, mice aged 12–14 weeks (Extended Data Fig. 5h) or 5–8 weeks (Fig. 4i–k and Extended Data Fig. 5j) were treated by intraperitoneal injection with 75 mg kg^{-1} tamoxifen in sunflower oil for five consecutive days. Four hours after the final tamoxifen injection, mice were infected with *C. rodentium*. Mice were grouped by genotype or by treatment with no randomization. The C57BL/6J female mice in Extended Data Fig. 5i were from the Jackson Laboratory and were eight weeks old at the time of infection.

C. rodentium were streaked out from glycerol stocks on MacConkey agar plates at 37 °C overnight. A single colony was inoculated into 10 ml Luria broth (LB) and grown on a shaker at 37 °C overnight. The overnight culture was diluted 1:100 and grown to log phase (optical density at 600 nm ($OD_{600\,nm}$) of around 0.5 after approximately three hours). Bacteria were collected by centrifugation at 6,000*g* for 15 min, washed twice with phosphate-buffered saline (PBS) and prepared for infection by equalization to 1×10^{10} CFUs per ml (1 $OD_{600\,nm}$ = 8×10^8 bacteria per ml). Mice were fasted for four hours and then dosed by oral gavage with 5×10^9 (Fig. 4i–k and Extended Data Fig. 5j) or 2×10^9 (Extended Data Fig. 5h,i) CFUs of *C. rodentium* (strains described below). Mice had access to food and water ad libitum after infection. At six or ten days after infection, mice were euthanized and gastrointestinal samples, including colon and caecum, were collected. Tissues were resected and splayed open, and the luminal contents were removed and resuspended in pre-weighted tubes containing 1 ml PBS. Tissues were later washed with PBS to remove non-adherent bacteria. Colon, caecum or spleen homogenate was plated on MacConkey agar containing 100 mg ml^{-1} streptomycin (Extended Data Fig. 4e) or LB agar containing nalidixic acid (Fig. 4e) to determine CFUs. Mice were picked and treated by the same individual, so blinding to genotype and treatment as well as during data collection and analysis was not possible. No statistical methods were used to predetermine sample size.

Intestinal permeability assay

Female *Rock1*$^{fl/fl}$*Rock2*$^{fl/fl}$ Villin.creERT2 mice and control Villin.creERT2 littermates, aged five to eight weeks, were administered tamoxifen intraperitoneally at a dose of 90 mg kg^{-1} in sunflower oil for five consecutive days. Mice underwent food restriction for 12 h before receiving a 600 mg kg^{-1} oral gavage of 4 kDa FITC–dextran. Four hours later, blood and faecal pellets were collected, and FITC fluorescence (485/528 nm ex/em) was measured.

Bacteria

EHEC O157:H7 EDL933 (ATCC700927) and *C. rodentium* DBS100 (ATCC51459) were obtained from the American Type Culture Collection (ATCC). A nalidixic-acid-resistant strain was derived from DBS100 by first growing 1 ml DBS100 overnight. The culture was centrifuged, resuspended in 100 µl PBS and plated on LB agar containing 30 µg ml^{-1} nalidixic acid. This resistant strain was used to generate the *nleL* mutant. The *E. coli* and *C. rodentium nleL* open reading frame (ORF) was replaced with a kanamycin resistance cassette from the pACYC177 vector using lambda red recombinase expressed by pKD46 (refs. 36,37). Gene replacement was verified by colony PCR (*E. coli ΔnleL::kanR*), and whole-genome sequencing (*C. rodentium* DBS100 WT and *C. rodentium* DBS100*ΔnleL::kanR*). The *C. rodentium* DBS100 WT assembly was generated using a combination of 75-bp paired-end Illumina reads and Oxford Nanopore Technologies long reads from isolate-derived total genomic DNA. The assembly and polishing of the combined long- and short-read data were performed using MicroPIPE v.0.9 (ref. 38). Illumina reads were mapped onto the *C. rodentium* DBS100 WT genome using GSNAP (v.2013-10-10)[39]. Single-nucleotide variants were detected using in-house R scripts, which used the Bioconductor packages GenomicRanges[40], GenomicAlignments[40] VariantTools and gmapR. Only base calls with a phred quality score of at least 30 were used for variant calling. Knockout of *nleL* was confirmed by visual inspection of read pile-ups using the Integrative Genomics Viewer[41]. Bacteria were transformed by electroporation with the pBR322-AmpR-dasherGFP plasmid[11] to visualize bacteria, and complementation of *C.r.ΔnleL::kanR* was achieved by transformation of the mutant strain with pBR322-GentR-nleL-COMP.

The primers used to generate recombineering insertions (5′ to 3′) include:

C.r.DBS100_NleLF1: ACAGGCAGAACTGGAGAATG

C.r.DBS100_NleLR1: GGGCGATTCAGGCCTGGTTTATCGCACTCCTTCTACTTAG

C.r.DBS100_NleLkanF1: CTAAGTAGAAGGAGTGCGATAAACCAGGCCTGAATCGCCC

C.r.DBS100_NleLkanR1: ATAATATTCATCTATGGTCTCTAAAACAACCAATTAACCAA

C.r.DBS100_NleLF2: TTGGTTAATTGGTTGTTTTAGAGACCATAGATGAATATTAT

C.r.DBS100_NleLR2: AATAACGAACATAATTTTCG

EDL933_NleLF1: TACAGGGACAGAAAGTTGTCC

EDL933_NleLR1: GGGCGATTCAGGCCTGGTAGAACTACAATGGCATAAAGAT

EDL933_NleLkanF1: ATCTTTATGCCATTGTAGTTCTACCAGGCCTGAATCGCCC

EDL933_NleLkanR1: ATAATATTCATCCATGGTCTCTAAAACAACCAATTAACCAA

EDL933_NleLF2: TTGGTTAATTGGTTGTTTTAGAGACCATGGATGAATATTAT

EDL933_NleLR2: TATGATTCTCCACGATTTGC

Outside primers to check insertion include:

C.r.DBS100_NleL_OUTF: GCTGGATGAAGTGGGCAGTGA

C.r.DBS100_NleL_OUTR: TCTCCACGATTTGTCCAG

EDL933_NleL_OUTF: AATCTGACATCTTATTTGTGGG

EDL933_NleL_OUTR: CTATAGTAACAAAAACATATTAATCTG

Cell culture

EA.hy926 (ATCC), 293T (ATCC), HT-29 (ATCC) and Caco-2 (ATCC) cells were cultured in Dulbecco's modified Eagle's high-glucose medium (DMEM) supplemented with 10 mM HEPES pH 7.4, 1× Glutamax (Gibco), 1× penicillin–streptomycin (Gibco), 1× non-essential amino acids (Gibco), 1 mM sodium pyruvate (Gibco) and 10% (v/v) fetal bovine serum (FBS, VWR) at 37 °C with 5% CO_2. Single-nucleotide polymorphism (SNP) profiles were compared with SNP calls from internal and external databases to determine or confirm ancestry. All cell lines tested negative for mycoplasma contamination before to storage or use at our institute.

For Caco-2 infections, bacteria were streaked from glycerol stocks onto trypticase soy agar (TSA) and used for experiments within one week. Caco-2 cells (3.5×10^5) were plated in six-well plates in antibiotic-free DMEM. On the same day, a single colony of the desired strain was grown at 37 °C overnight in 5 ml terrific broth (TB). Overnight cultures were diluted 1:50 in TB and grown until bacteria reached an

$OD_{600\,nm}$ of 0.6–0.8. Bacteria were pelleted at 3,000*g*, washed with PBS and then incubated in fresh PBS at room temperature for 15 min. After one further wash with PBS, bacteria were resuspended in DMEM without supplements. Caco-2 cells were infected with an MOI of 25 (1 $OD_{600\,nm}$ = 8×10^8 bacteria per ml) by centrifugation at 1,000*g* for 10 min.

Intestinal organoids from C57BL/6J mice, or *Rock1*$^{fl/fl}$*Rock2*$^{fl/fl}$ Villin.creERT2 mice and control Villin.creERT2 mice, were generated as described[35]. After 2–15 passages, organoids were disrupted into single-cell suspensions. IEC monolayers were established by seeding 50,000–60,000 cells into translucent 24-well Matrigel-coated transwell inserts with a pore size of 0.4 µm in organoid medium[42] (L-WRN conditioned supernatant, 10 µm Y-27632 (MedChemExpress) and 50 ng ml^{-1} mEGF (Thermo Fisher Scientific)). Cultures were grown for ten days. For ERT2-Cre induction, cells were treated 48 h before the experiment with 250 nM 4-OHT. Transwells were transitioned to antibiotic-free medium without Y-27632 the day before infection. Monolayers were infected with *C. rodentium* (WT or Δ*nleL*) in the exponential growth phase at an MOI of 0.25. After four hours, the medium was changed to prevent the overgrowth of non-adherent bacteria. After a further 16 h, the cells were treated with 10 µg ml^{-1} PI (or 50 nM SYTOX green) for 30 min, washed with PBS and then fixed in 4% paraformaldehyde for 10 min. The fixed cells were permeabilized with 0.2% Triton X-100 and stained with 4′,6-diamidino-2-phenylindole (DAPI) and 0.165 µM AF647–phalloidin (Thermo Fisher Scientific).

IEC monolayers for experiments with FlaTox were grown identically and Y-27632 was removed 24 h before FlaTox treatment. For Villin.creERT2 monolayers, 250 nM 4-OHT was administered 48 h before stimulation. Monolayers were administered 2 mg ml^{-1} anthrax lethal factor N terminus fused to *Legionella pneumophila* flagellin (LFn-FlaA)[34], 4 mg ml^{-1} protective antigen[34] (PA) and 10 µg ml^{-1} PI (or 50 nM SYTOX green). The medium contained 10 µM Y-27632 or 2.5 mM cytochalasin D (Sigma) as indicated. Monolayers were fixed after 30 min and stained with DAPI as described above. For imaging, transwell membranes were cut out with a razor blade, placed on a microscopy slide, layered with Vectashield hardening mounting medium and coverslipped.

For transparent monolayers, TrypLE-dissociated organoids were seeded on Matrigel-covered 96-well tissue culture plates at 30,000 cells per well in 50% L-WRN conditioned supernatant containing 3 µM CHIR99021 (Cayman Chemical) and 10 µM Y-27632 (MedChemExpress)[43]. Twenty-four hours later, the medium was changed to antibiotic-free L-WRN with 3 µM CHIR99021 without Y-27632. Forty-eight hours later, monolayers were infected with 1×10^4 *C. rodentium* *ΔnleL* or *ΔnleL* + pNleL after overnight culture and redilution for exponential growth. Plates were spun at 300*g* for 10 min to help with epithelial attachment of bacteria and then incubated overnight at 37 °C and 5% CO_2. After 11 h of infection, the wells were washed once with warm PBS and new medium was added containing 1 µg ml^{-1} PI.

IEC imaging and cell-extrusion analysis

Fixed IEC monolayers on transwells were imaged on an inverted Leica SP8 confocal microscope using a 40× oil (numerical aperture 1.3) objective. Imaging parameters on the Leica LAS X (v.3.7.5) software were set to acquire DAPI, PI, SYTOX green and GFP (bacteria). Three-dimensional (3D) confocal *z*-stacks were acquired using Nyquist sampling rates. Six to seven fields of view were acquired for each sample. The 3D datasets were processed and analysed using the Imaris Spots tool to quantify cellular extrusion levels. In brief, a Gaussian blur image filter was first applied to all channels to reduce background noise. Afterwards, the Imaris Spots tool was used to segment and isolate DAPI- and PI-positive or SYTOX-green-positive cells (PI^+DAPI+ or $SYTOX^+DAPI^+$) from the 3D image stacks. A low threshold intensity was set for the PI and SYTOX channel so that both infected and uninfected cells were segmented using the Imaris Spots tool. After segmentation, the shortest distance metric in Imaris was used to calculate the distance between the centroids of a PI^+ or $SYTOX^+$ spot and the closest $DAPI^+$ spot. A batch Imaris run to segment spots of $DAPI^+$ and PI^+ or $SYTOX^+$ cells was performed using identical segmentation parameters. The shortest distance metric was then extracted and used for quantification of the cell-extrusion analysis of all samples. Bacteria exhibiting GFP signals were filtered out by segmenting and masking them using a pixel classifier in Imaris. After this masking procedure, the shortest distance between SYTOX-green-positive cells and DAPI-positive cells was measured to analyse extrusion events, as detailed above.

For live imaging of transparent monolayers, plates were imaged for two hours in a live imaging set-up (Celldiscoverer 7), recording oblique/bright-field and red fluorescence with a Hammamastu Orca Flash 4.0 camera. Images were taken using the 5×/0.35 NA objective with the addition of the 2× optovar. Images were collected on the Celldiscoverer 7 in intervals of 60 s with the exposure and light source intensity of oblique and red channels set at 5 ms and 15%, and 50 ms and 30%, respectively. Focus was maintained throughout the time-lapse using the Zeiss definite focus system. Extrusion was quantified in a blinded manner, by recording the time from the first noticeable changes in cell shape to the finished extrusion of PI-positive cells in the bright-field/oblique channel.

IL-18 enzyme-linked immunosorbent assay (ELISA)

One hundred microlitres of medium from transwell infection experiments, collected immediately before infected monolayers were fixed for microscopy, was analysed with mouse IL-18 DuoSet ELISA (R&D Systems DY7625-05) according to the manufacturer's instructions and quantified using a standard curve. Untreated medium background was subtracted.

CytoTox-Glo viability assay

Twenty-five microlitres of supernatant medium, collected immediately before infected monolayers were fixed for microscopy, was mixed with 12.5 µl of CytoTox-Glo reagent (Promega) and incubated for 15 min at room temperature. The luminescence was assessed as per the manufacturer's recommendations. Untreated medium background was subtracted.

Transepithelial electrical resistance assay

Medium was exchanged on monolayers on the day of infection and they were allowed to equilibrate for 20 min at room temperature. Transepithelial resistance was recorded in each transwell with an epithelial voltohmmeter (EVOM2, World Precision Instruments). The background resistance of an empty transwell with medium was subtracted.

Plasmids and lentiviral vectors

The genetically barcoded *E. coli* effector library was maintained in the lentiviral vector pMIN-ducer (Genscript). cDNAs encoding N-terminal 3×Flag-NleL, NleL(C753A), the PPR domain (amino acids (aa) 135–371), or the NEL domain (aa 372–782) were expressed using pMIN-ducer or pCDNA3.1Hygro(+) (Genscript). cDNAs encoding Myc–GST-tagged CARDs (Extended Data Table 2) were cloned into pCDNA3.1:Zeo(+) (Genscript). cDNAs encoding C-terminal Rho-1D4-tagged caspase-1, caspase-4 or caspase-1/4 CARD swap chimeras (aa 1–80, 1–10, 6–15, 11–20, 16–25 and 21–30) were cloned into pCDNA3.1Hygro(+) (Genscript). cDNAs encoding C-terminal Rho-1D4-tagged ROCK1, ROCK2, ROCK2ΔPH (aa 1–1,141), ROCK2-PH (aa 1,142–1,354) and C-terminal truncations (20 aa from Δ20–240) were cloned into pCDNA3.1Hygro(+) (Genscript). For transient expression in 293T cells, 3×10^6 cells were plated in 10-cm dishes and transfected the next day with 3 µg of pCDNA3.1Zeo(+) total plasmid DNA using Lipofectamine 2000 (Thermo Fisher Scientific). Proteins were expressed for 24 h before being collected for downstream manipulations.

For lentiviral packaging, 2.5×10^6 293T cells in 10-cm plates were transfected with 5 µg pMIN-ducer, 10 µg pCMV-Δ8.9 and 0.5 µg pCMV-VSVG (1:2.3:0.2 mole ratio). Virus-containing supernatants

were collected after 72 h, passed through 0.45-µm syringe filters and used immediately for infection of EA.hy926, Caco-2 or HT-29 cells (2×10^5 cells seeded into six-well plates the previous day). Virus was supplemented with 10 µg ml^{-1} polybrene (Millipore) during infections. After 48 h, transduced cells were selected with 4 µg ml^{-1} puromycin (Takara). Mock-infected cells were used to judge selection duration and efficiency.

Positive selection screen

The lentiviral library was packaged using 12 15-cm plates of 293T cells. Each plate (2.7×10^7 cells) was transfected with 50.8 µg DNA (library plasmid, pCMV-Δ8.9 and pCMV-VSVG plasmids at a molar ratio of 1:2:0.2) using Lipofectamine 2000 reagent (Thermo Fisher Scientific). At six hours after transfection, the medium containing the transfection mix was replaced with fresh medium supplemented with 1 U ml^{-1} DNase I, 5 mM $MgCl_2$ and 20 mM HEPES pH 7.2. After overnight culture at 37 °C, this medium was replaced with fresh medium. After another 24 h, the lentivirus-containing medium was collected, pooled, passed through a 0.45 µm filter and concentrated by ultracentrifugation (Thermo Fisher Scientific, S50-A fixed angle rotor, 100,000*g*). Concentrated lentivirus was resuspended in PBS containing 1% bovine serum albumin (BSA) and aliquots were stored at −80 °C.

EA.hy926 cells were infected at an MOI of 0.3 to ensure a single integrant frequency of 97% with 1,000-fold coverage. On day 1, EA.hy926 cells were seeded into two 10-cm plates (1.2×10^6 cells each). On day 2, cells were infected with lentivirus diluted in DMEM supplemented with 10 µg ml^{-1} polybrene (Millipore). On day 3, virus-containing medium was replaced with fresh DMEM. On day 4, cells were expanded into a 15-cm plate. On day 5, antibiotic selection was initiated with DMEM containing 2 µg ml^{-1} puromycin (Takara). After a further five days, cells were expanded into four 15-cm plates with antibiotic-free DMEM, and cultured for two days.

For LPS screens, EA.hy926 containing the *E. coli* effector library were seeded into six 15-cm plates (1.5×10^6 cells per plate). *E. coli* effectors were induced with 250 ng ml^{-1} doxycycline for 48 h. For each plate, cells were lifted with TrypLE Express (Thermo Fisher Scientific), washed with PBS, resuspended in 110 µl Buffer R (Neon, Thermo Fisher Scientific) and electroporated (three plates with and three plates without 7 µg LPS) using the Neon Transfection System 100 µl kit. Electroporated cells were washed with PBS and plated in six-well dishes containing fresh DMEM. Electroporated control cells were passaged until LPS-electroporated cells recovered. After 11 days, genomic DNA was isolated from LPS-resistant and control cells using the Gentra Puregene Cell kit (QIAGEN). The barcoded regions were amplified by PCR and then sequenced by next-generation sequencing.

Next-generation sequencing and analysis

For submitted PCR amplicons, 40 ng DNA was used to generate sequencing libraries with the KAPA HyperPrep kit (Roche) that incorporated custom adapters and library amplification PCR primers from Integrated DNA Technologies. Amplicon libraries were quantified and the average library size was determined using the NGS Fragment kit in Fragment Analyzer (Agilent Technologies). Libraries were pooled and the Qubit dsDNA HS Assay kit (Thermo Fisher Scientific) was used to quantify the pool. Library pools were sequenced on a HiSeq 2500 (Illumina) to generate a minimum of three million paired-end 75-base-pair reads for each sample. A sample ORF matrix was generated by counting exact matches of ORF barcodes in the sample FASTQ files. The count matrix was normalized by library-size-based factors. Differentially enriched ORFs were identified using DESeq2 (ref. 44) by comparing LPS-treated cells with control cells.

Cell assays

For EA.hy926 cell death assays, 8×10^3 cells per well were seeded into 96-well plates. The following day, cells were treated with 250 ng ml^{-1} doxycycline (Takara). After a further 24 h, cells were transfected with ultra-pure *E. coli* O111:B4 LPS (0.5 µg per well, InvivoGen) using Lipofectamine LTX transfection reagent (0.2 µl per well, Thermo Fisher Scientific), or treated with 25 µM Val-boroPro (Millipore) for 24 h. LDH release was measured by CytoTox Non-radioactive Cytotoxicity Assay (Promega). Cells were cultured with the membrane-impermeable nuclear dye YOYO-1 (Thermo Fisher Scientific) to determine the kinetics of cell death. Cells were imaged every 30 min for 24 h in an IncuCyte S3 (Essen BioScience, 10× objective). Nuclear-ID (Enzo) was added to cultures after the last time point to quantify total cell numbers. Image quantification was performed using Incucyte Base Analysis software. Results were plotted as the percentage of YOYO-1$^+$ cells within the total population.

Immunoblotting and immunoprecipitation

Cells were washed with PBS and lysed in RIPA buffer (25 mM Tris HCl pH 7.6, 150 mM NaCl, 1% NP-40, 1% sodium deoxycholate and 0.1% SDS) supplemented with protease inhibitors (Halt, Thermo Fisher Scientific). Lysates were clarified by centrifugation at 20,000*g* for 30 min. For immunoprecipitation, soluble lysates were incubated with 20 µl Flag-M2–sepharose (MilliporeSigma), Rho-1D4–sepharose (Rho-1D4 Ab, University of British Columbia, coupled to cyanogen bromide-activated sepharose beads, GE Healthcare) or GST–sepharose (MilliporeSigma) for one hour at 4 °C. Beads were washed with lysis buffer, and captured proteins were eluted with 100 µg ml^{-1} 3×Flag peptide (MilliporeSigma), 10 mM reduced glutathione peptide (MilliporeSigma) or 250 µM Rho-1D4 peptide (TETSQVAPA, Genscript) overnight at 4 °C.

Antibodies

Antibodies recognized actin (clone C4, MP Bio, 0.1 µg ml^{-1}), β-tubulin (ab15568, abcam, 0.1 µg ml^{-1}), Myc tag (9B11, Cell Signaling Technology, 1 µg ml^{-1}), Flag epitope (M2-HRP, Sigma-Aldrich, 1 µg ml^{-1}) ROCK1 (Cell Signaling Technology, 1 µg ml^{-1}), ROCK2 (Cell Signaling Technology, 1 µg ml^{-1}), phospho-MLC2 (Cell Signaling Technology, 1 µg ml^{-1}), p66β (Bethyl, 1 µg ml^{-1}), Rho-1D4 (Novus, 1 µg ml^{-1}), ubiquitin (VU-1, LifeSensors, 1 µg ml^{-1}), K11-linked polyubiquitin[45], K48-linked polyubiquitin[46] and K63-linked polyubiquitin[46] (1 µg ml^{-1}).

Identification of NleL substrates

Proteomic analyses were performed on EA.hy926 expressing doxycycline-inducible 3×Flag-NleL. Cells were treated with doxycycline for zero, one, two, four or six hours (in duplicate except for the one-hour treatment), and collected by scraping into 50 mM HEPES pH 8.5, 9 M urea, 150 mM NaCl and protease inhibitors (Roche). Lysates were rotated end-over-end at room temperature for one hour, and then centrifuged at 15,000*g* for 20 min. Soluble lysate containing 20 mg protein was reduced (5 mM dithiothreitol (DTT), 45 min at 37 °C), alkylated (15 mM iodoacetamide (IAA), 20 min at room temperature in the dark) and quenched (5 mM DTT, 15 min at room temperature in the dark). Proteins were pelleted by chloroform–methanol precipitation, resuspended in 8 M urea, 20 mM HEPES, pH 8.0, diluted to 4 M urea and digested for four hours at 37 °C with lysyl endopeptidase (Wako) at an enzyme-to-protein ratio of 1:100. The sample was diluted further to 1.3 M urea and subjected to overnight enzymatic digestion at 37 °C with sequencing-grade trypsin (Promega) at an enzyme-to-protein ratio of 1:50. The peptides were acidified with 20% trifluoroacetic acid (TFA, final concentration 1%), centrifuged at 18,000*g* for 15 min and desalted using a Sep-Pak C_{18} column (Waters).

Approximately 500 µg of eluted peptides from each treatment was lyophilized and reserved for global proteome abundance. The remaining eluted peptides were lyophilized and used for K-ε-GG analysis. For global proteome samples, 100 µg of peptides from each sample was dissolved in 20 mM HEPES pH 8.0 at 1 mg ml^{-1}. Isobaric labelling was performed using TMT11-plex reagents (Thermo Fisher Scientific).

Each unit (0.8 mg) of TMT reagent was allowed to reach room temperature immediately before use, pelleted in a benchtop centrifuge and resuspended with occasional vortexing in 41 µl anhydrous acetonitrile (ACN) before mixing with peptides (29% final ACN concentration). After incubation at room temperature for one hour, the reaction was quenched for 15 min with 20 µl of 5% hydroxylamine. Labelled peptides were combined in equimolar ratios and dried. The TMT-labelled sample was re-dissolved in 80 µl 0.1% TFA and centrifuged at 16,000*g*, and the supernatant was processed further. Offline high-pH reversed-phase fractionation was performed on a 1100 HPLC system (Agilent) using an ammonium formate buffer system. Peptides (400 µg) were loaded onto a 2.1 × 150 mm, 3.5-µm 300 Extend-C_{18} Zorbax column (Agilent) and separated over a 75-min gradient from 5% to 85% ACN into 96 fractions (flow rate = 200 µl per min). The fractions were concatenated into 24 fractions, mixing different parts of the gradient to produce samples that would be orthogonal to downstream low pH reversed-phase LC–MS/MS. Fractions were dried and desalted using C_{18} stage-tips as described[47]. Peptides were lyophilized and resuspended in buffer A (2% ACN and 0.1% formic acid) for LC–MS/MS analysis.

For quantification of K-ε-GG peptides, lyophilized peptides were reconstituted in 1× detergent containing IAP buffer (Cell Signaling Technology) for immunoaffinity enrichment. Enrichment for K-ε-GG peptides was performed at 4 °C on a MEA2 automated purification system (PhyNexus) using 1 ml PhyTips (PhyNexus) packed with 20 µl ProPlus resin coupled to 200 µg of anti-K-ε-GG (Cell Signaling Technology) antibody. PhyTip columns were equilibrated for two cycles (one cycle = aspiration and dispensing, 0.9 ml, 0.5 ml min^{-1}) with 1 ml 1× IAP buffer before contact with peptides. PhyTip columns were incubated with peptides for 16 cycles of capture, followed by 6 cycles of wash, twice with 1 ml 1× IAP buffer and 4 times with 1 ml water. Captured peptides were eluted with 60 µl 0.15% TFA in eight cycles in which the volume aspirated or dispensed was adjusted to 60 µl. Enriched ubiquitylated peptides were prepared as described[48]. Labelled peptides were combined, dried and resolubilized in 0.15% TFA for high-pH reversed-phase fractionation using a commercially available kit (Thermo Fisher Scientific). Fractionation was performed with a modified elution scheme in which 11 fractions were collected (F1, 13.5% ACN; F2, 15% ACN; F3, 16.25% ACN; F4, 17.5 ACN; F5, 20% ACN; F6, 21.5% ACN; F7, 22.5% ACN; F8, 23.75% ACN; F9, 25% ACN; F10, 27.5% ACN; and F11, 30% ACN) and then combined into 6 fractions (F1 + F6, F2 + F7, F8, F3 + F9, F4 + F10 and F5 + F11). Peptides were lyophilized and resuspended in 10 µl buffer A for LC–MS/MS analysis.

Mass spectrometry

LC–MS/MS analysis was performed by injecting 5 µl of each fraction on an Orbitrap Lumos mass spectrometer (Thermo Fisher Scientific) coupled to a Dionex Ultimate 3000 RSLC (Thermo Fisher Scientific) using a 25-cm IonOpticks Aurora Series column (IonOpticks) with a gradient of 2% to 30% buffer B (98% ACN, 2% H_2O with 0.1% FA, flow rate = 300 nl per min). All samples were analysed with a total run time of 180 min. The Orbitrap Lumos collected FTMS1 scans at 120,000 resolution with an AGC target of 1×10^6 and a maximum injection time of 50 ms. FTMS2 scans on precursors with charge states of 3–6 were collected at 15,000 resolution with CID fragmentation at a normalized collision energy of 35%, an AGC target of 2×10^4 (proteome) or 2×10^5 (K-ε-GG) and a max injection time of 100 ms (proteome) or 200 ms (K-ε-GG). Synchronous precursor selection (SPS) MS3 scans were analysed in the Orbitrap at 50,000 resolution with the top eight most intense ions in the MS2 spectrum subjected to HCD fragmentation at a normalized collision energy of 55%, an AGC target of 2×10^5 and a max injection time of 100 ms (proteome) or 350 ms (K-ε-GG).

MS data were searched using Mascot against a concatenated target–decoy human database (downloaded August 2017) containing common contaminant sequences, and the protein sequence of *E. coli* NleL ligase with a precursor mass tolerance of 50 ppm, 0.8 Da fragment ion tolerance and tryptic specificity up to 2 (proteome) or 3 missed cleavages (K-ε-GG). For global proteome analysis, the following modifications were considered: carbamidomethyl cysteine (+57.0214), TMT-labelled N terminus (+229.1629) and TMT-labelled lysine (+229.1629) as static modifications, and oxidized methionine (+15.9949) and TMT-labelled tyrosine (+229.1629) as variable modifications. For analysis of K-ε-GG peptides, TMT-labelled diglycine-modified lysine (+343.2059) was also included as a variable modification. Peptide spectral matches for each run were filtered using linear discriminant analysis to an FDR of 2% and subsequently in aggregate to a protein-level FDR of 2%. TMT-MS3 quantification was performed using Mojave, and only peptide-spectrum matches (PSMs) that had isolation specificities greater than or equal to 0.5 were considered for the final dataset. The abundance of ubiquitylation on each peptide or each identified protein was estimated by using a model fitted with Tukey median polish summarization with imputation of missing values below a censoring threshold of 28. For each pairwise comparison, the change in abundance (log_2 'fold' values) and the results of an ANOVA test were reported. We used the implementation of these methods in MSstats v.3.16.0 (ref. 49). Data were further processed in R to produce figures.

Protein expression and purification

E. coli NleL S170-R782 WT/C357A constructs were expressed as N-terminal His fusion constructs in *E. coli* Rosetta 2 (Millipore). Bacterial cell pellets were frozen and stored at −80 °C. Cells were resuspended in lysis buffer (50 mM Tris pH 8.0, 200 mM NaCl, 5 % glycerol, 5 mM $MgCl_2$, 1 mM TCEP or 2 mM 2-mercaptoethanol, plus protease inhibitors (Roche), DNase and lysozyme) and lysed by microfluidization, and the lysate was clarified by centrifugation at 20,000*g* for one hour. The soluble lysate was passed through a 2-µm filter. NTA Superflow resin (QUIAGEN) or TALON Superflow (GE Healthcare) were used for affinity purification. The resin was incubated with the clarified lysate at 4 °C for one hour and then washed with up to 2 l of wash buffer (50 mM Tris pH 8.0, 200 mM NaCl, 5 % glycerol and 1 mM TCEP or 2 mM 2-mercaptoethanol). Proteins were eluted in wash buffer supplemented with 250 mM imidazole pH 8.0 (Sigma). NleL proteins were concentrated and purified by size-exclusion chromatography using a Superdex 200 column (GE Healthcare) pre-equilibrated with 50 mM Tris pH 8.0, 300 mM NaCl, 5% glycerol and 1 mM TCEP. Pure-protein-containing fractions were pooled, concentrated and stored at −80 °C.

C-terminal 1D4-tagged human caspase-4 (full length 1–377), human ROCK1 (full length 1–1,354) and human ROCK2 (full length 1–1,388, kinase domain 1–409, PH domain 1,142–1,388) were purified from 293T cells. Cell pellets were resuspended in 10 mM HEPES pH 7.4, 150 mM NaCl, 10% glycerol, 1 mM $MgCl_2$, 1 mM TCEP containing protease inhibitor cocktail (Halt) and benzonase. Lysates were clarified by centrifugation at 20,000*g* for 30 min at 4 °C. 1D4–sepharose was used for purification. Lysates were incubated with resin for one hour at 4 °C and washed three times with lysis buffer. Proteins were eluted with 25 µM 1D4 peptide in 10 mM HEPES pH 7.4, 150 mM NaCl, 10% glycerol, 1 mM $MgCl_2$ and 1 mM TCEP.

In vitro ubiquitylation assays

Reactions contained 2.5 ng $µl^{-1}$ human E1 enzyme (Boston Biochem), 0.125 µg $µl^{-1}$ ubiquitin (Boston Biochem), 0.01 µg $µl^{-1}$ Ube2D3 (Boston Biochem), 0.01 µg $µl^{-1}$ NleL, 0.1 µg $µl^{-1}$ human caspase-4, ROCK1 or ROCK2, 50 mM Tris pH 8.0, 50 mM NaCl, 5 mM $MgCl_2$ and 0.1 mM DTT. Reactions were initiated with 5 mM ATP, incubated at 37 °C and quenched with LDS sample loading buffer (Thermo Fisher Scientific).

Statistics

P value calculations for the mass spectrometry analyses in Fig. 2a are described above. All other statistical analyses were performed using GraphPad Prism v.9 and v.10.4.2.

Reporting summary

Further information on research design is available in the Nature Portfolio Reporting Summary linked to this article.

Data availability

Raw data for the whole-genome sequencing of *C. rodentium* have been deposited in the Sequence Read Archive (PRJNA1150236). Proteomics data have been deposited to MassIVE (MSV000095663).

36. Datsenko, K. A. & Wanner, B. L. One-step inactivation of chromosomal genes in *Escherichia coli* K-12 using PCR products. *Proc. Natl Acad. Sci. USA* **97**, 6640–6645 (2000).
37. Heckman, K. L. & Pease, L. R. Gene splicing and mutagenesis by PCR-driven overlap extension. *Nat. Protoc.* **2**, 924–932 (2007).
38. Murigneux, V. et al. MicroPIPE: validating an end-to-end workflow for high-quality complete bacterial genome construction. *BMC Genomics* **22**, 474 (2021).
39. Wu, T. D. & Nacu, S. Fast and SNP-tolerant detection of complex variants and splicing in short reads. *Bioinformatics* **26**, 873–881 (2010).
40. Lawrence, M. et al. Software for computing and annotating genomic ranges. *PLoS Comput. Biol.* **9**, e1003118 (2013).
41. Robinson, J. T. et al. Integrative genomics viewer. *Nat. Biotechnol.* **29**, 24–26 (2011).
42. Miyoshi, H. & Stappenbeck, T. S. In vitro expansion and genetic modification of gastrointestinal stem cells in spheroid culture. *Nat. Protoc.* **8**, 2471–2482 (2013).
43. Geiser, P., van Rijn, J. M. & Sellin, M. E. Time-lapse imaging of inflammasome-dependent cell death and extrusion in enteroid-derived intestinal epithelial monolayers. *Methods Mol. Biol.* **2641**, 203–221 (2023).
44. Love, M. I., Huber, W. & Anders, S. Moderated estimation of fold change and dispersion for RNA-seq data with DESeq2. *Genome Biol* **15**, 550 (2014).
45. Matsumoto, M. L. et al. K11-linked polyubiquitination in cell cycle control revealed by a K11 linkage-specific antibody. *Mol. Cell* **39**, 477–484 (2010).
46. Newton, K. et al. Ubiquitin chain editing revealed by polyubiquitin linkage-specific antibodies. *Cell* **134**, 668–678 (2008).
47. Rappsilber, J., Mann, M. & Ishihama, Y. Protocol for micro-purification, enrichment, pre-fractionation and storage of peptides for proteomics using StageTips. *Nat. Protoc.* **2**, 1896–1906 (2007).
48. Rose, C. M. et al. Highly multiplexed quantitative mass spectrometry analysis of ubiquitylomes. *Cell Syst.* **3**, 395–403.e4 (2016).
49. Choi, M. et al. MSstats: an R package for statistical analysis of quantitative mass spectrometry-based proteomic experiments. *Bioinformatics* **30**, 2524–2526 (2014).

Acknowledgements We thank members of the V.M.D. and I.R. laboratories for advice, discussions and reagents, and L. Carfrae for necropsy assistance. We acknowledge technical assistance from staff in the OHSU Advanced Light Microscopy shared resource. This work was supported by NIH grants to I.R. (AI167974-01) and M.V.M. (5T32AI170496-02).

Author contributions G.L., I.R., N.K., K.N. and V.M.D. designed experiments. G.L., I.R., M.V.M., R.M.P., W.P.S., E.M.K., H.Z. and A.G.J. performed experiments. Y.L. managed lentiviral packaging of *E. coli* ORFs. R.R. analysed the results of the positive selection screen. T.K.C. performed mass spectrometry under the supervision of C.M.R. E.M.K., A.G.J. and M.W.T. generated bacterial strains. E.S. characterized bacterial strains by whole-genome sequencing. P.K. imaged and designed methods for analysing organoids. G.L. and K.N. wrote the paper with input from all co-authors.

Competing interests All authors except I.R., M.V.M., R.M.P. and W.P.S. are employees of Genentech. The remaining authors declare no competing interests.

Additional information

Supplementary information The online version contains supplementary material available at https://doi.org/10.1038/s41586-025-09645-0.

Correspondence and requests for materials should be addressed to Giovanni Luchetti, Isabella Rauch or Vishva M. Dixit.

Peer review information *Nature* thanks the anonymous reviewers for their contribution to the peer review of this work.

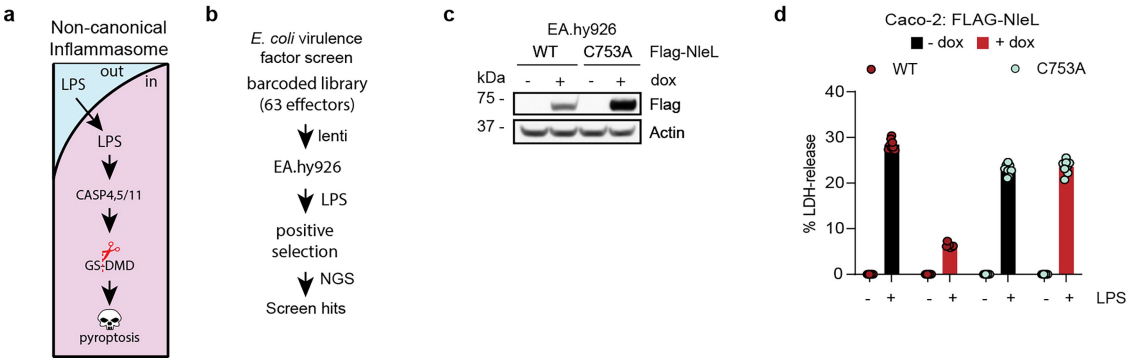

Extended Data Fig. 1 | Screening for inhibitors of pyroptosis induced by intracellular LPS. a, The non-canonical inflammasome pathway. **b**, Positive selection screen strategy. NGS, next-generation sequencing. **c**, Immunoblots of EA.hy926 cells expressing doxycycline (dox)-inducible NleL. Cells were treated with dox for 24 h. Results representative of 3 independent experiments. **d**, Percentage of LDH released from Caco-2 cells after LPS transfection. Bars represent the mean of 8 separate wells. For gel source data, see Supplementary Fig. 1.

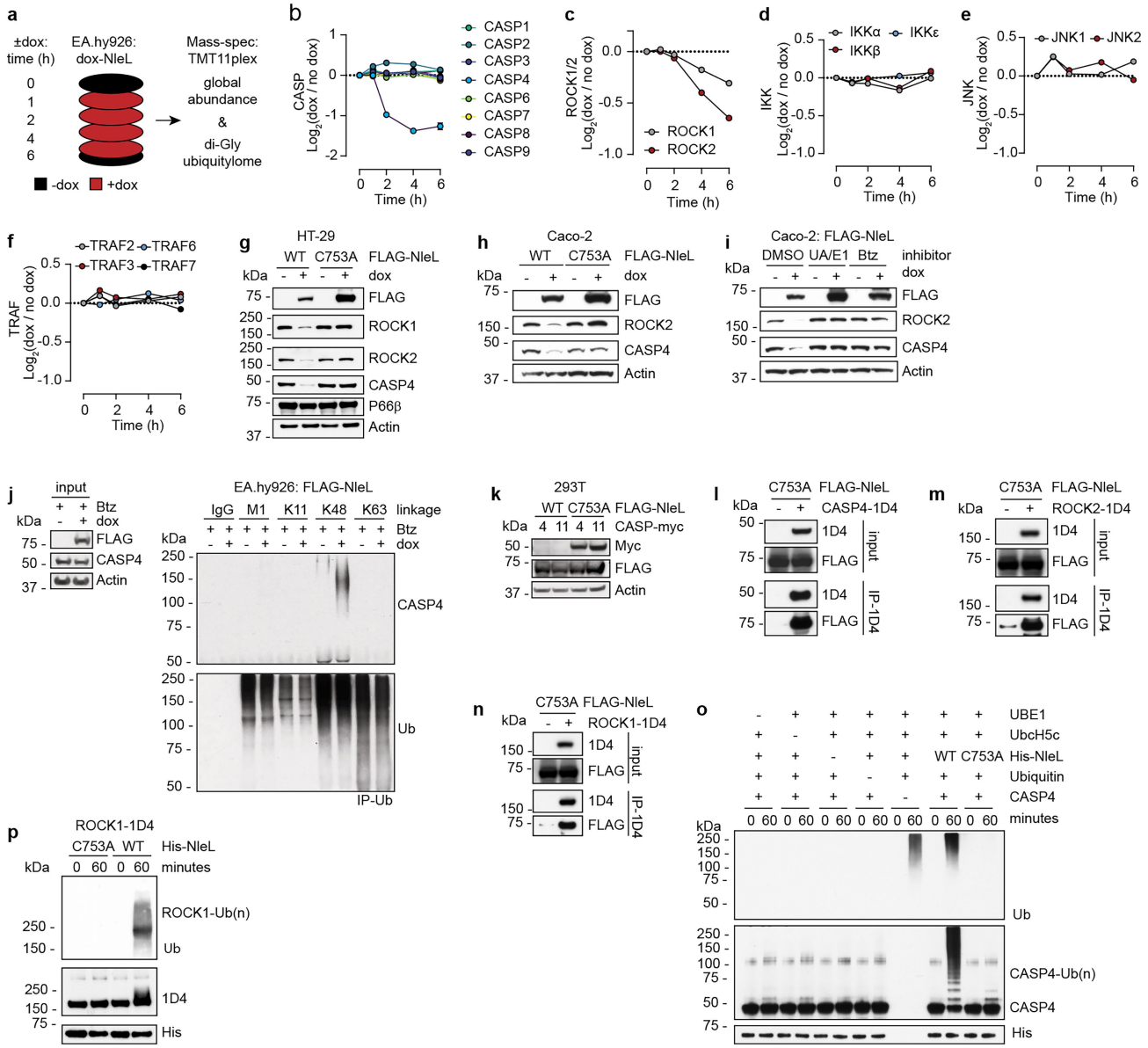

Extended Data Fig. 2 | Caspase-4, ROCK1 and ROCK2 are direct targets of NleL. a, Proteomics strategy to identify NleL substrates in EA.hy926 cells. **b**–**f**, Changes in the abundance of caspases (**b**), ROCK1 and ROCK2 (**c**), IKKs (**d**), JNK1 and JNK2 (**e**) and TRAF proteins (**f**) after doxycycline (dox)-induced NleL expression in EA.hy926 cells. Circles represent the mean of 2 biological replicates. **g**–**i**, Immunoblots of HT-29 (**g**) and Caco-2 cells (**h**,**i**) transfected with Flag-NleL. Results representative of 3 independent experiments. **j**, Immunoblots of ubiquitylated proteins immunoprecipitated from EA.hy926 cells with linkage-specific anti-ubiquitin (Ub) antibodies or an IgG isotype control. Results representative of 3 independent experiments. **k**, Immunoblots of 293T cells transfected with Flag-NleL and myc-caspases. Results representative of 3 independent experiments. **l**–**n**, Immunoblots of caspase-4 (**l**), ROCK2 (**m**) or ROCK1 complexes (**n**) immunoprecipitated from transfected 293T cells. Results representative of 3 independent experiments. **o**,**p**, Immunoblots of in vitro ubiquitylation reactions using caspase-4 (**o**) or ROCK1 (**p**) as the NleL substrate. Results representative of 3 independent experiments. For gel source data, see Supplementary Fig. 1.

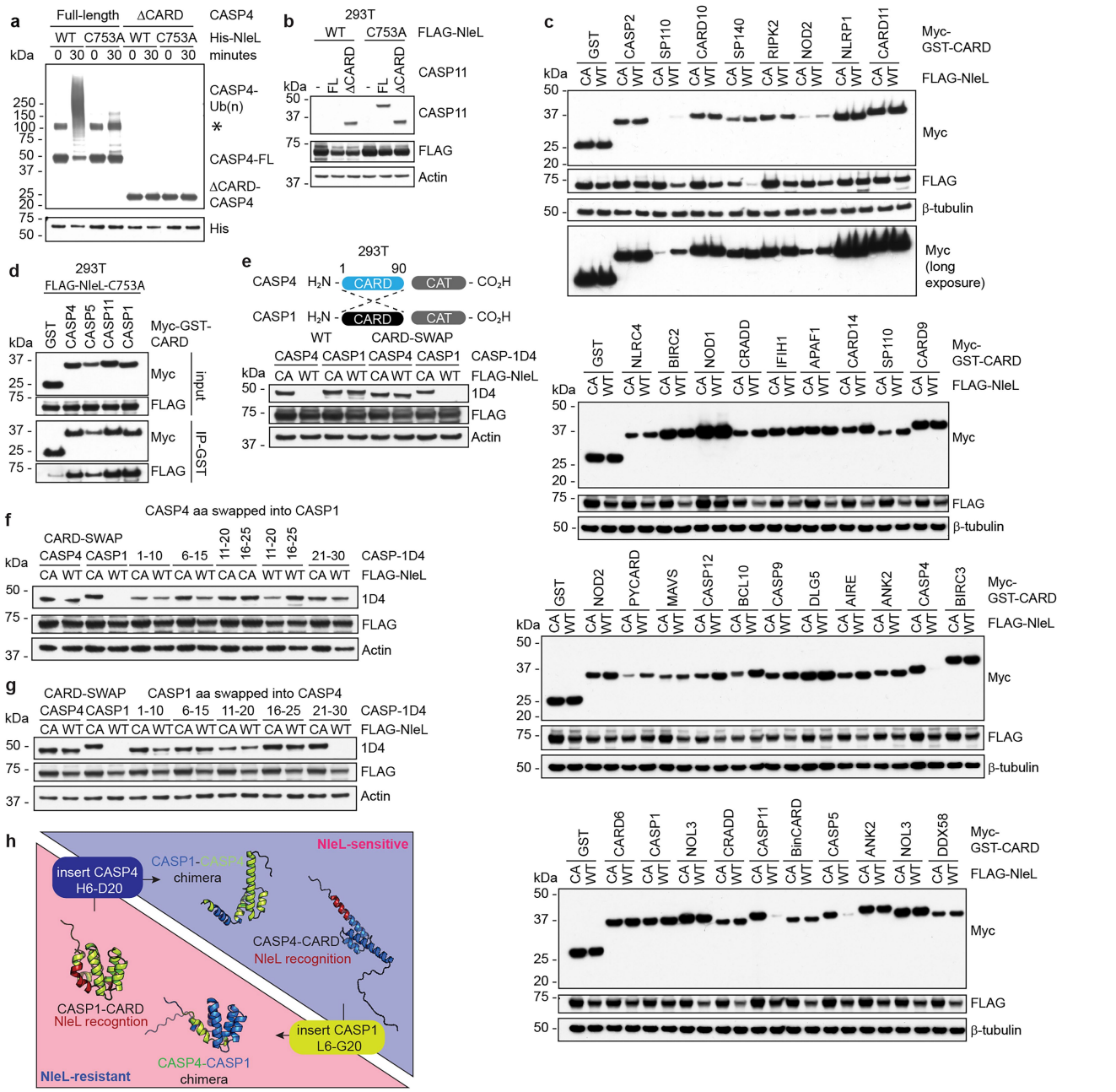

Extended Data Fig. 3 | NleL targets the LPS-sensing CARD of caspase-1, caspase-4 and caspase-5. a, Immunoblots of in vitro ubiquitylation reactions. Asterisk indicates dimeric caspase-4. Results representative of 3 independent experiments. **b**,**c**,**e**–**g**, Immunoblots of transfected 293T cells. CA, NleL(C753A). In **c**, only the CARDs of the indicated proteins were co-expressed with NleL. CARD boundaries are defined in Extended Data Table 2. Results representative of 3 independent experiments. **d**, Immunoblots of CARD complexes immunoprecipitated from transfected 293T cells. Results representative of 3 independent experiments. **h**, AlphaFold-predicted structural models of the caspase-1 CARD, caspase-4 CARD, and chimeric caspase-1/4 CARDs with their corresponding sensitivity to NleL. The minimal regions determining NleL resistance or sensitivity are coloured red. The caspase-1 CARD contains the six antiparallel helices characteristic of death-fold proteins, whereas the caspase-4 CARD does not. Chimeric CARDs may adopt intermediate folds that are structurally homologous to the inserted donor sequences from either caspase-1 (H6-D20, blue) or caspase-4 (L6-G20, green). For gel source data, see Supplementary Fig. 1.

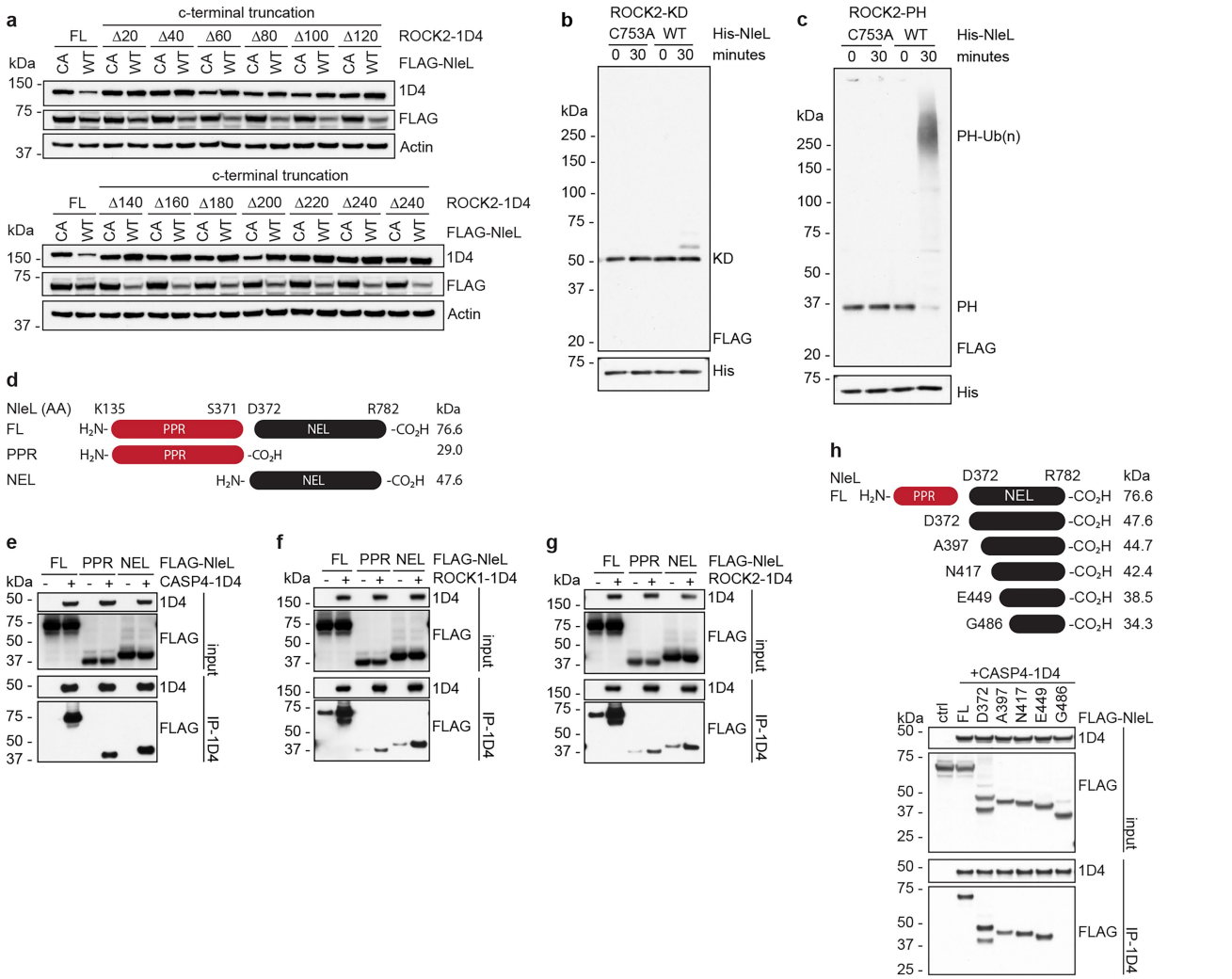

Extended Data Fig. 4 | NleL targets the ROCK2 PH domain. a, Immunoblots of 293T cells co-expressing NleL and ROCK2 (full-length [FL] or truncated at the C-terminus by the indicated number of residues). Results representative of 3 independent experiments. **b**,**c**, Immunoblots of in vitro ubiquitylation reactions with NleL on ROCK2 domains (kinase domain (KD) (**b**); pleckstrin homology domain (PH) (**c**)). Results representative of 3 independent experiments. **d**, Truncation mutants of NleL used in **e**–**g**, pentapeptide repeat (PPR) and novel E3 ligase domain (NEL). **e**–**h**, Immunoblots of caspase-4 (**e**,**h**), ROCK1 (**f**) or ROCK2 complexes (**g**) with NleL truncation mutants immunoprecipitated from transfected 293T cells. Immunoblots **e**–**g** use FL NleL from the same immunoblot as Extended Data Fig. 2l–m. Results representative of 3 independent experiments. For gel source data, see Supplementary Fig. 1.

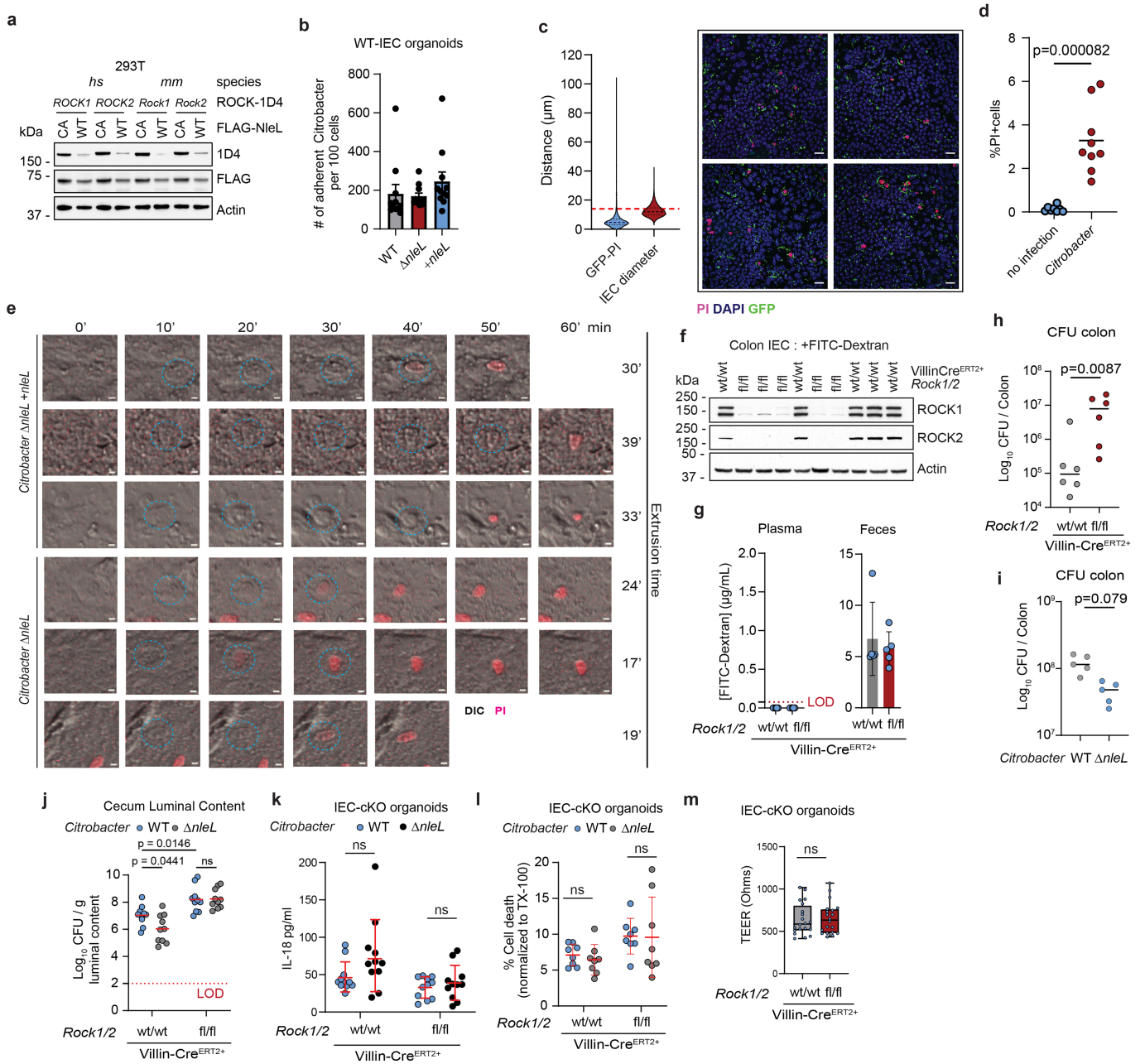

Extended Data Fig. 5 | IEC expulsion from monolayers is ROCK dependent and sensitive to NleL. a, Immunoblots of 293T cells transfected with human or mouse ROCK1/2 and NleL. Results representative of 3 independent experiments. **b**, Number of GFP-expressing Citrobacter bacteria adhered to WT IEC monolayers. Data are mean ± s.d. Circles, a single image field (n = 11 per condition taken from n = 4 monolayers per group). *P* values determined by one-way ANOVA. **c**, Average distance of GFP+ bacteria from nearest PI+ nucleus, compared to epithelial cell diameter, related to transwell monolayer data in Fig. 4g. n = 12 monolayers with representative images demonstrating bacterial infection of PI+ cells. Scale bar is 20 µm. **d**, Quantification of % PI+ cells among all cells in uninfected versus *Citrobacter* strain DBS100 WT infected monolayers. Circles, single image field (no infection, n = 8 and *Citrobacter* n = 9) from 3 separate monolayers. *P* values determined by two-tailed Mann–Whitney test. Results representative of 3 independent experiments. **e**, Extrusion imaging of individual cells in live-imaged monolayers infected with *Citrobacter* strain DBS100 (Δ*nleL* or +*nleL*). Representative frames from imaging data used for quantification in Fig. 4h. Blue circles mark extruding cell analysed from start to finish. Scale bar = 5 µm. Results representative of 2 independent experiments. **f**, Immunoblot of IECs collected from individual mice in (g). **g**, FITC–dextran concentration in plasma and faeces. Circles, individual mice (n = 5 mice per group). Data are mean ± s.d. of 3 independent experiments. **h–j**, CFUs in the colons (**h**,**i**), and caecum lumens (**j**) of mice infected with *Citrobacter* strain DBS100 WT or Δ*nleL* for 10 (**h**) or 6 days (**i**,**j**). Circles, individual mice (**h**,**i** n = 5 mice per group, **j**, data pooled from 2 experiments, n = 10 mice per group, LOD=limit of detection). Lines indicate the mean. *P* values determined by two-way ANOVA. **k**,**l**, Secreted IL-18 (**k**) or cell death (**l**) from IECs infected by *Citrobacter* Δ*nleL* or +NleL in Fig. 4m. Circles, individual transwells of IEC organoids (**k**, n = 11 and **l**, n = 8). Data are mean ± s.d. *P* values determined by two-tailed Mann–Whitney test. Results representative of 3 independent experiments. **m**, Transepithelial electrical resistance in transwells (circles, n = 20) of IEC organoids. Box plot shows the median, interquartile range and minimum to maximum values (whiskers). *P* values determined by two-tailed Mann–Whitney test. Results representative of 3 independent experiments. For gel source data, see Supplementary Fig. 1.

Extended Data Table 1 | *E.* coli effector library

ORF #	ORF.Name	NCBI.Accession	ORF #	ORF.Name	NCBI.Accession
1	espO1-1	260844437	33	nleH1	NP_286534
2	espO1-2	260868027	34	nleH1-1	209398763
3	espZ	215488982	35	nleH2	NP_287959
4	sepZ	260845700	36	nleB2	NP_286532
5	sepZ/espZ	NP_290271	37	nleB2-2	260843011
6	nleG2-3	209396587	38	nleB1	NP_289553
7	cesT	NP_290260	39	nleC	NP_286533
8	espH	NP_290264	40	espW	NP_289177
9	nleE2	215486207	41	espR4	NP_288396
10	espT	CAX32470	42	espR3	NP_288394
11	espY2	NP_285765	43	espFu/tccP	NP_288437
12	nleF	NP_287958	44	espG2	215487973
13	nleG-3	209400919	45	espG1	215489001
14	nleG2-2	260843013	46	espG	NP_290289
15	nleG	215486170	47	nleA	EIQ72111
16	espM2	NP_289175	48	espR1	NP_287686
17	espM1	NP_287949	49	espX5	NP_290699
18	map	NP_290262	50	nleA/espI	NP_287961
19	nleG6-2	254793092	51	espK	NP_287316
20	nleG6-1	387506605	52	espX1	NP_285716
21	nleG-1	260845677	53	espY3	NP_286160
22	nleG7	NP_287535	54	espX4	NP_290672
23	nleG7	260847263	55	espL2	NP_289551
24	nleG8-2	260844213	56	espL1	NP_288154
25	espJ	NP_288436	57	espX7/nleL	NP_287310
26	nleE1	215488273	58	espX2	NP_286562
27	nleE	NP_289554	59	espL4	NP_290644
28	nleD	NP_286535	60	espX6	NP_290952
29	espF	NP_290250	61	espX7	15830814
30	tccP2	260844510	62	espY4	NP_290352
31	espY1	NP_285753	63	espN	NP_287312
32	cif	AAN07916			

Extended Data Table 2 | Myc–GST–CARD constructs

construct	Symbol
1	GST control
2	AIRE
3	ANK2
4	APAF1
5	BCL10
6	BinCARD
7	BIRC2
8	BIRC3
9	CARD10
10	CARD11
11	CARD14
12	CARD6
13	CARD9
14	CASP1
15	CASP11
16	CASP12
17	CASP2
18	CASP4
19	CASP5
20	CASP9
21	CRADD
22	DDX58
23	DLG5
24	IFIH1
25	MAVS
26	NLRC4
27	NLRP1
28	NOD1
29	NOD2
30	NOL3
31	PYCARD
32	RIPK2
33	SP110
34	SP140

nature portfolio

Corresponding author(s): Giovanni Luchetti, Isabella Rauch, Vishva M. Dixit

Last updated by author(s): 09.08.2025

Reporting Summary

Nature Portfolio wishes to improve the reproducibility of the work that we publish. This form provides structure for consistency and transparency in reporting. For further information on Nature Portfolio policies, see our Editorial Policies and the Editorial Policy Checklist.

Please do not complete any field with "not applicable" or n/a. Refer to the help text for what text to use if an item is not relevant to your study.
For final submission: please carefully check your responses for accuracy; you will not be able to make changes later.

Statistics

For all statistical analyses, confirm that the following items are present in the figure legend, table legend, main text, or Methods section.

n/a	Confirmed	
☐	X	The exact sample size (*n*) for each experimental group/condition, given as a discrete number and unit of measurement
☐	X	A statement on whether measurements were taken from distinct samples or whether the same sample was measured repeatedly
☐	X	The statistical test(s) used AND whether they are one- or two-sided *Only common tests should be described solely by name; describe more complex techniques in the Methods section.*
X	☐	A description of all covariates tested
X	☐	A description of any assumptions or corrections, such as tests of normality and adjustment for multiple comparisons
☐	X	A full description of the statistical parameters including central tendency (e.g. means) or other basic estimates (e.g. regression coefficient) AND variation (e.g. standard deviation) or associated estimates of uncertainty (e.g. confidence intervals)
☐	X	For null hypothesis testing, the test statistic (e.g. *F*, *t*, *r*) with confidence intervals, effect sizes, degrees of freedom and *P* value noted *Give P values as exact values whenever suitable.*
X	☐	For Bayesian analysis, information on the choice of priors and Markov chain Monte Carlo settings
X	☐	For hierarchical and complex designs, identification of the appropriate level for tests and full reporting of outcomes
X	☐	Estimates of effect sizes (e.g. Cohen's *d*, Pearson's *r*), indicating how they were calculated

Our web collection on statistics for biologists contains articles on many of the points above.

Software and code

Policy information about availability of computer code

Data collection	Imaging data (live and fixed) were analyzed with Imaris 10.2 and IncuCyte S3 2020B
Data analysis	Mass spectrometry data analyzed using Mascot 2.4.1 and MSstats 3.16.0. NGS data were analyzed using DESeq2. Plots were generated with Prism v.9 & v.10.4.2

For manuscripts utilizing custom algorithms or software that are central to the research but not yet described in published literature, software must be made available to editors and reviewers. We strongly encourage code deposition in a community repository (e.g. GitHub). See the Nature Portfolio guidelines for submitting code & software for further information.

Data

Policy information about availability of data

All manuscripts must include a data availability statement. This statement should provide the following information, where applicable:

- Accession codes, unique identifiers, or web links for publicly available datasets
- A description of any restrictions on data availability
- For clinical datasets or third party data, please ensure that the statement adheres to our policy

Raw data for Citrobacter whole-genome sequencing are deposited to Sequence Read Archive (PRJNA1150236), Proetomics deposted to MASSive (MSV000095663). Source data for Figs. 1-4 and Extended Data Figs. 1-5 are provided with the paper.

Research involving human participants, their data, or biological material

Policy information about studies with human participants or human data. See also policy information about sex, gender (identity/presentation), and sexual orientation and race, ethnicity and racism.

Reporting on sex and gender	N/A
Reporting on race, ethnicity, or other socially relevant groupings	N/A
Population characteristics	N/A
Recruitment	N/A
Ethics oversight	N/A

Note that full information on the approval of the study protocol must also be provided in the manuscript.

Field-specific reporting

Please select the one below that is the best fit for your research. If you are not sure, read the appropriate sections before making your selection.

[x] Life sciences [ ] Behavioural & social sciences [ ] Ecological, evolutionary & environmental sciences

For a reference copy of the document with all sections, see nature.com/documents/nr-reporting-summary-flat.pdf

Life sciences study design

All studies must disclose on these points even when the disclosure is negative.

Sample size	No sample size calculations were performed. The *C. rodentium* infection model is well-established and highly reproducible (Nat Protoc. 2016 Oct;11(10): 1851-76. doi: 10.1038/nprot.2016.100). For our primary readout, we relied on bacterial burden, typically measured in feces or tissue samples through colony-forming unit (CFU) analysis, which is known for producing consistent and tightly grouped data. Based on previous studies, an average group size of 4 (Sci Rep. 2017 Sep 21;7(1):12099. doi: 10.1038/s41598-017-12256-z) to 5 (Nature. 2024 May;629(8012):669-678. doi: 10.1038/s41586-024-07288-1. Epub 2024 Apr 10) animals has been shown to yield reliable and statistically robust results for this outcome.
Data exclusions	No data were excluded from the analysis
Replication	For in vivo experiments, readouts were performed with 5 animals per genotype, and all attempts at replication were successful. For in vitro experiments, readouts were performed with 3 or greater biological replicates, and all attempts at replication were successful. In both cases, experiments were repeated independently at least 3 times.
Randomization	Groups were determined by genotype rather than treatment, therefore, randomization was not applicable.
Blinding	Imaging was performed blindly and automatically using a Leica Confocal or Incucyte system. For other experiments, mice and cell lines were picked and treated by the same individual, so blinding to genotype and treatment as well as during data collection and analysis was not possible.

Reporting for specific materials, systems and methods

We require information from authors about some types of materials, experimental systems and methods used in many studies. Here, indicate whether each material, system or method listed is relevant to your study. If you are not sure if a list item applies to your research, read the appropriate section before selecting a response.

Materials & experimental systems

n/a	Involved in the study
☐	☒ Antibodies
☐	☒ Eukaryotic cell lines
☒	☐ Palaeontology and archaeology
☐	☒ Animals and other organisms
☒	☐ Clinical data
☒	☐ Dual use research of concern
☒	☐ Plants

Methods

n/a	Involved in the study
☒	☐ ChIP-seq
☒	☐ Flow cytometry
☒	☐ MRI-based neuroimaging

Antibodies

Antibodies used

Antibodies used for western blots were from Genentech (anti-K11-linked; anti-K48-linked; and anti-63-linked polyubiquitin antibodies were used at 1 ug/mL), Cell Signaling Technology (anti-myc cat#2276, used at 1 ug/mL; anti-ROCK1 cat#4035 used at 1 ug/mL; anti-ROCK2 cat#8236 used at 1 ug/mL; anti-PARP cat#9542 used at 1 ug/mL; anti-phospho-MLC2 cat#3671 used at 1 ug/mL), Abcam (anti-beta tubulin cat#ab15568 used at 0.1 ug/mL), Bethyl (anti-P66beta cat#A301-281A-T used at 1 ug/mL), MPBio (anti-actin cat#0869100-CF used 0.1 ug/mL), Novus (anti-Rho1D4 cat#NBP1-47602 used at 1 ug/mL), SigmaAldrich (anti-FLAG M2 HRP cat#A8592 used at 1 ug/mL), and Lifesensors (anti-ubiquitin cat#VU101 used at 1 ug/mL).

Validation

-anti-K11-linked; anti-K48-linked; and anti-63-linked polyubiquitin antibodies was validated previously by Matsumoto, M. L. et al. (2010) and Newton, K. et al (2008).
-9B11 anti-myc (Cell Signaling Technology, cat#2276, lot 24). The antibody guarantee covers the use of the antibody for WB applications. The antibody has been referenced in 2422 publications.
-C8F7 anti-ROCK1 (Cell Signaling Technology, cat#4035, lot 3). The antibody guarantee covers the use of the antibody for WB applications. The antibody was verified in our study showing WB depletion in ROCK1/2 deficient mice Figure 4l and Extended Data Figure 5f.
-anti-ROCK2 (Cell Signaling Technology, cat#8236, lot 2). The antibody guarantee covers the use of the antibody for WB applications. The antibody was verified in our study showing WB depletion in ROCK1/2 deficient mice Figure 4l and Extended Data Figure 5f.
-anti-PARP (Cell Signaling Technology, cat #9542, lot 15). The antibody guarantee covers the use of the antibody for WB applications. The antibody has been referenced in 4458 publications.
-anti-phospho-MLC2 (Cell Signaling Technology, cat#3671, lot 6). The antibody guarantee covers the use of the antibody for WB applications. The antibody has been referenced in 828 publications.
-anti-beta Tubulin (Abcam, cat#ab15568, lot GR3237077-10). The antibody guarantee covers the use of the antibody for WB applications. The antibody has been referenced in 101 publications.
-C4 anti-actin (MPbio, cat#0869100-CF, lot QR14180). The antibody guarantee covers the use of the antibody for WB applications. The antibody has been referenced in 1215 publications.
-anti-P66-beta (Bethyl, cat#A301-281A-T, lot 1). The antibody guarantee covers the use of the antibody for WB applications. The antibody has been referenced in 5 publications.
-anti-Rho1D4 (Novus, cat#NBP1-47602, lot 1006). The antibody has been validated previously by Molday, R.S. et al (2014).
-anti-FLAG M2 HRP (SigmaAldrich, cat#A8592, lot 1006). The antibody guarantee covers the use of the antibody for WB applications. The antibody has been referenced in 1904 publications.
-VU-1 anti-ubiquitin (Lifesensors, cat#VU101, lot not available). The antibody guarantee covers the use of the antibody for WB applications. The antibody has been verified with di-ubiquitin standards by the vendor. Reactivity is independent of species due to the high conservation of ubiquitin across eukaryotes.

Eukaryotic cell lines

Policy information about cell lines and Sex and Gender in Research

Cell line source(s)	293T (ATCC CRL-3216), Caco-2 (ATCC HTB-37), Ea.hy926 (ATCC CRL-922), HT-29 (ATCC HTB-38)
Authentication	Cells not authenticated
Mycoplasma contamination	Cells are negative for mycoplasma
Commonly misidentified lines (See ICLAC register)	not used

Palaeontology and Archaeology

Specimen provenance	
Specimen deposition	
Dating methods	

☐ Tick this box to confirm that the raw and calibrated dates are available in the paper or in Supplementary Information.

Ethics oversight	

Note that full information on the approval of the study protocol must also be provided in the manuscript.

Animals and other research organisms

Policy information about studies involving animals; ARRIVE guidelines recommended for reporting animal research, and Sex and Gender in Research

Laboratory animals	All mice (Mus musculus) were maintained on a C57BL/6N genetic background. Strains included Villen.CreERT2 Rock1 wt/wt Rock2 wt/wt and VillenCreERT2 Rock1 fl/fl Rock2 fl/fl (Sambandam, A. et al 2023. heliyon.2023.e14238). For C. rodentium studies, female mice were aged 12-14 weeks (Extendend Data Fig. 5h) or 5-8 weeks (Fig. 4 i-k and Extended Data Fig. 5j). Mice were housed in individually ventilated cages within animal rooms maintained on a 14:10-hour, light-dark cycle. Animal rooms were temperature and humidity-controlled, between 68-79°F and 30-70% respectively, with 10 to 15 room air exchanges per hour.
Wild animals	The study did not use wild animals
Reporting on sex	Female mice were used in all experiments.
Field-collected samples	The study did not involve samples collected from the field.
Ethics oversight	All mouse studies complied with relevant ethics regulations and were approved by either the Genentech Institutional Animal Care and Use Committee (IACUC) in an Association for Assessment and Accreditation of Laboratory Animal Care (AAALAC)-accredited facility or by the Oregon Health and Science University IACUC.

Note that full information on the approval of the study protocol must also be provided in the manuscript.

No	Yes	
☐	☐	Public health
☐	☐	National security
☐	☐	Crops and/or livestock
☐	☐	Ecosystems
☐	☐	Any other significant area

Experiments of concern

Does the work involve any of these experiments of concern:

No	Yes	
☐	☐	Demonstrate how to render a vaccine ineffective
☐	☐	Confer resistance to therapeutically useful antibiotics or antiviral agents
☐	☐	Enhance the virulence of a pathogen or render a nonpathogen virulent
☐	☐	Increase transmissibility of a pathogen
☐	☐	Alter the host range of a pathogen
☐	☐	Enable evasion of diagnostic/detection modalities
☐	☐	Enable the weaponization of a biological agent or toxin
☐	☐	Any other potentially harmful combination of experiments and agents

Plants

Seed stocks

Novel plant genotypes

Authentication

ChIP-seq

Data deposition

☐ Confirm that both raw and final processed data have been deposited in a public database such as GEO.

☐ Confirm that you have deposited or provided access to graph files (e.g. BED files) for the called peaks.

Data access links
May remain private before publication.

Files in database submission

Genome browser session
(e.g. UCSC)

Methodology

Replicates

Sequencing depth

Antibodies

Peak calling parameters

Data quality

Software

Flow Cytometry

Plots

Confirm that:

☐ The axis labels state the marker and fluorochrome used (e.g. CD4-FITC).

☐ The axis scales are clearly visible. Include numbers along axes only for bottom left plot of group (a 'group' is an analysis of identical markers).

☐ All plots are contour plots with outliers or pseudocolor plots.

☐ A numerical value for number of cells or percentage (with statistics) is provided.

Methodology

Sample preparation

Instrument

Software

Cell population abundance

Gating strategy

☐ Tick this box to confirm that a figure exemplifying the gating strategy is provided in the Supplementary Information.

Magnetic resonance imaging

Experimental design

Design type

Design specifications

Behavioral performance measures

Imaging type(s)

Field strength

Sequence & imaging parameters

Area of acquisition

Diffusion MRI ☐ Used ☐ Not used

Preprocessing

Preprocessing software

Normalization

Normalization template

Noise and artifact removal

Volume censoring

Statistical modeling & inference

Model type and settings

Effect(s) tested

Specify type of analysis: ☐ Whole brain ☐ ROI-based ☐ Both

Statistic type for inference

(See Eklund et al. 2016)

Correction

Models & analysis

n/a	Involved in the study
☐	☐ Functional and/or effective connectivity
☐	☐ Graph analysis
☐	☐ Multivariate modeling or predictive analysis

Functional and/or effective connectivity

Graph analysis

Multivariate modeling and predictive analysis

09/08/2025

Giovanni Luchetti